minerals

MDPI

Article

A Combined EPMA and LA-ICP-MS Investigation on Bi-Cu-Au Mineralization from the Kizhnica Ore Field (Vardar Zone, Kosovo)

Sławomir Mederski [1,*], Jaroslav Pršek [1,*], Dimitrina Dimitrova [2] and Bahri Hyseni [3]

[1] Faculty of Geology, Geophysics, and Environmental Protection, AGH UST, 30 Mickiewicz Av., 30-059 Krakow, Poland
[2] Geological Institute, Bulgarian Academy of Sciences, 1113 Sofia, Bulgaria; didi@geology.bas.bg
[3] Faculty of Geosciences, University of Mitrovica "Isa Boletini", Ukshin Kovacica, 40000 Mitrovica, Kosovo; bahri.hyseni2013@gmail.com
* Correspondence: mederski@agh.edu.pl (S.M.); prsek@yahoo.com (J.P.)

Abstract: This paper describes a newly discovered Bi-Cu ± Au mineralization co-occurring with Pb-Zn-Ag hydrothermal mineralization within the Kizhnica-Hajvalia-Badovc ore field, central Kosovo, Vardar Zone. The mineralogy of two styles of Bi-Cu ± Au mineralization was described using EPMA in combination with reflected and transmitted light microscopy. Hydrothermal Cu-Bi veinlets in the Kizhnica andesite quarry consist of Bi sulfosalts (bismuthinite, cosalite, aikinite, and krupkaite), pyrite, hematite, chalcopyrite, galena, sphalerite, and tetrahedrite group minerals. Disseminated Bi-Au-Cu-Te mineralization from the contact type of mineralization (hornfels) consists of Bi sulfosalts (cannizzarite, bismuthinite, galenobismutite, cosalite), associated with sulfarsenides (arsenopyrite, gersdorffite, and cobaltite), base metal sulfides (chalcopyrite, pyrite, sphalerite, pyrrhotite, and galena), native gold, native bismuth, and tetradymite. LA-ICP-MS analyses of sphalerite, chalcopyrite, and tetrahedrite indicate increased content of In and Sn in the Kizhnica Bi-Cu-Au mineralizing system, while LA-ICP-MS analyses in pyrites show the presence of many elements, e.g., Au, As, Co, Sb, Tl, Hg, Pb, Bi related to the structure of pyrite or controlled by nano-inclusions. The results suggest a connection between Bi-Cu±Au mineralization and the proximity to intrusive rocks, which may be helpful for Au exploration in Kosovo.

Keywords: Kizhnica ore field; hornfels; epithermal; bismuth sulfosalts; sulfarsenides; gold

Citation: Mederski, S.; Pršek, J.; Dimitrova, S.; Hyseni, B. A Combined EPMA and LA-ICP-MS Investigation on Bi-Cu-Au Mineralization from the Kizhnica Ore Field (Vardar Zone, Kosovo). *Minerals* **2021**, *11*, 1223. https://doi.org/10.3390/min11111223

Academic Editors: Lucie Mathieu, Michel Jébrak, Nadia Mohammadi

Received: 20 September 2021
Accepted: 1 November 2021
Published: 3 November 2021

1. Introduction

The Serbo-Macedonian metallogenic province (SMMP), part of the Western Tethyan metallogenic belt [1], is dominated by Pb-Zn-Ag deposits [2–5]. However, Tertiary Cu-Au rich deposits are also observed in the area: porphyry systems of Oligocene-Miocene age (Skouries, Illovitza, Bučim, and Tulare), carbonate replacement deposits (Olympias and Piavitsa), and the Plavica high-sulfidation epithermal deposit [6–10]. In the SMMP, Bi mineralization is ubiquitous and occurs as minor constituents in both Pb-Zn-Ag and Cu-Au-rich systems and is associated with skarn, porphyry, epithermal, carbonate-replacement, and shear-zone related occurrences [11–16]. Furthermore, within the SMMP, the coexistence and spatial relationship between both Pb-Zn-Ag and Bi-Au±Cu systems depends on the distance from the intrusive complex, which are also the main source of hydrothermal fluids [17].

One of the most neglected areas of the SMMP in terms of detailed metallogenic studies is the Trepça Mineral Belt (TMB) in Kosovo. This area is known for the occurrence of many Pb-Zn-Ag deposits (e.g., the famous Stan Terg Pb-Zn-Ag deposit); moreover, it is highly prospective for finding new resources of Bi-Au ± Cu that are rarely

reported in the literature. Bismuth, Au, and Cu mineralization in the TMB occur in close proximity to intrusive rocks compared with more distal position of the Pb-Zn-Ag mineralization, which will be discussed in this manuscript. One of the areas where such situation has been recognized is the Kizhnica ore field, where the newly discovered Bi-Cu-Au mineralization co-occurs with Pb-Zn-Ag.

Bismuth-copper-gold paragenesis in Kosovo is known from only a few deposits and mineral occurrences [15,16,18–21], likely due to an insufficient number of prospecting projects or a focus strictly on Pb-Zn-Ag mineralization. Bismuth sulfosalts with native Au were reported in the Stan Terg (also known as Stari Trg, Stan Trg, or Trepča) Pb-Zn-Ag deposit by Kołodziejczyk et al. [15,16] and occur in galena-rich skarn mineralization as well as in arsenopyrite-rich skarn-free vein-type mineralization. Close to Stan Terg, two locations with Bi-Cu-Au mineralization were described in the Mazhiq area. Hydrothermal veins in volcanic rocks, with paragenesis containing Bi sulfosalts, chalcopyrite, pyrite, and native gold were identified there [19,21], in addition to mineralized carbonate metasomatic-veins in listvenites (altered ultramafic rocks) with Bi sulfosalts in association with Ni-Fe sulfarsenides, galena, and native gold [20,21]. Gold and bismuth mineralization is also known from the Slivovo Au-Ag deposit, a few kilometers east of the Kizhnica ore field, where they occur within hornfels and skarns [18].

Reflected and transmitted light microscopy, EPMA, and LA-ICP-MS were used to determine the mineralogy, mineral chemistry, and paragenetic relations of Bi sulfosalts, various sulfides, sulfarsenides, and associated Bi-Au-Te bearing minerals from two newly discovered styles of Bi-Cu-Au mineralization: epithermal veinlets from the Kizhnica andesite quarry and Bi-Au-Cu-Te mineralization from hornfels north of the quarry. The results give new insights into the presence, extent, characteristics, and prospecting potential of the Bi-Au±Cu mineralization in Kosovo.

2. Geological Setting

2.1. Trepça Mineral Belt

The Kizhnica-Hajvalia-Badovc ore field is located in central Kosovo, about 10 km SE of the capital city—Prishtina. The Pb-Zn-Ag deposits of the Kizhnica area are located in the southern part of the Trepça Mineral Belt (TMB), which hosts numerous polymetallic deposits and occurrences (Figure 1). The TMB is part of the Serbo-Macedonian metallogenic province and is located within the central part of the Vardar Zone, in the vicinity of the Kopaonik granite massif, between the Serbo-Macedonian Massif to the east and the Dinarides to the west (Figure 1). The polymetallic mineralization in the TMB is of the Oligocene-Miocene age, has a hydrothermal origin, and is related to post-collisional magmatic activity [22–24]. This part of the Vardar zone is composed of metamorphosed rocks of Paleozoic and Triassic age, Jurassic ophiolite complex (consisting mainly of serpentinite and gabbro with an admixture of sedimentary rocks), and Jurassic and Cretaceous sedimentary complex (series of flysch, carbonate rocks, as well as volcanic and volcanoclastic rocks). Tertiary rocks are represented by andesites, trachytes, latites, and felsic pyroclastic rocks [24–26]. The polymetallic mineralization in the TMB is controlled by three NNW-trending regional fault zones (I) Batlava-Artana Zone, (II) Belo Brdo-Stan Terg-Hajvalia Zone, and (III) Crnac Zone (Figure 1).

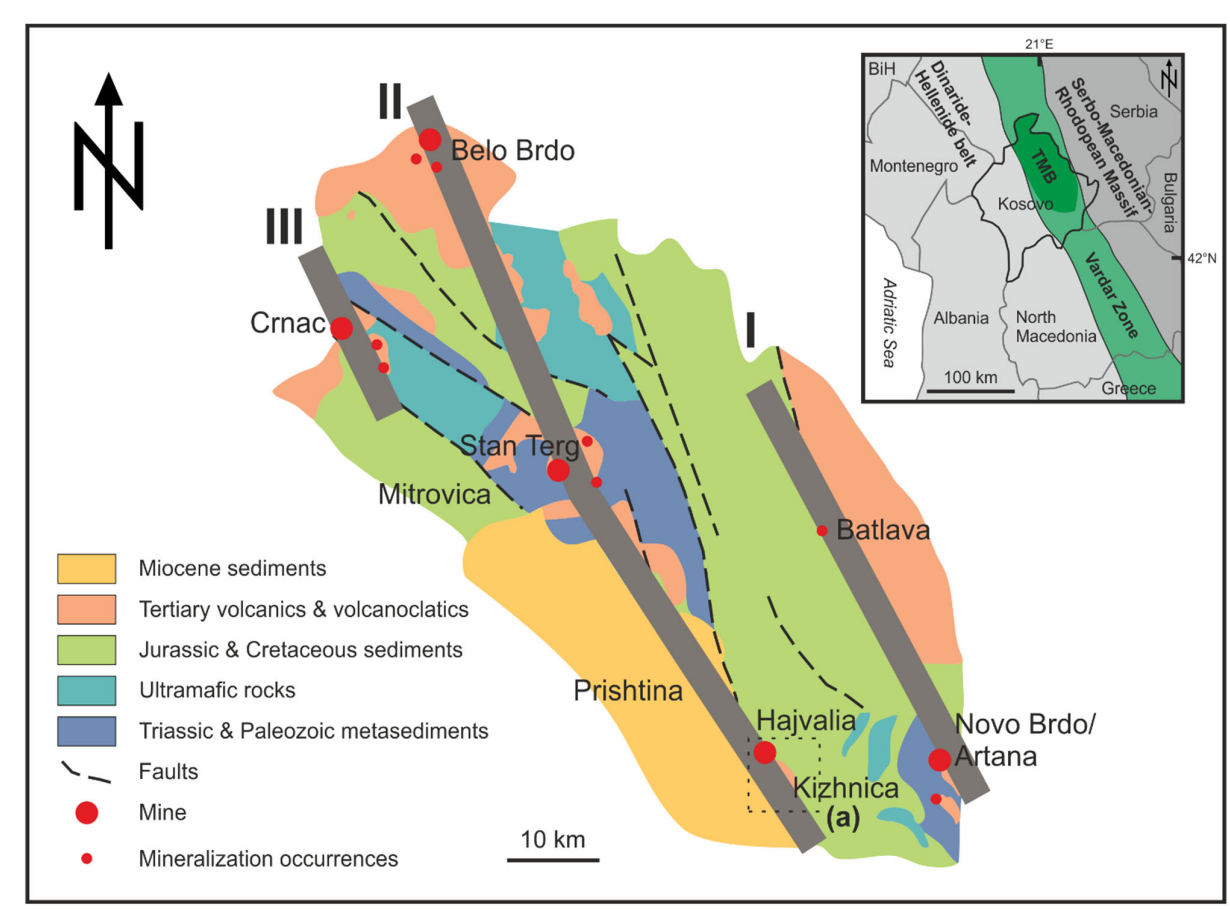

Figure 1. Simplified geological map of the Vardar Zone and the Trepça Mineral Belt (TMB), modified after [23,24]. Abbreviations: I = Batlava-Artana Zone; II = Belo Brdo-Stan Terg-Hajvalia Zone; III = Crnac Zone; a = Kizhnica-Hajvalia-Badovc ore field.

The most important Pb-Zn-Ag deposits in the TMB are the Stan Terg, Artana, Hajvalia, Kizhnica, Belo Brdo, Crnac, and Drazhnje (Batlava) (Figure 1). The Oligocene-Miocene mineralization is hosted by carbonate rocks, volcanic rocks, serpentinites, and schists. Due to the diverse lithological units intersected by the major tectonic zones providing pathway for hydrothermal fluids, as well as different temperature conditions and the nature of the fluids, various styles of polymetallic mineralization are observed in Kosovo, such as skarns, carbonate replacement (manto-like replacement ore bodies), veins, breccias, and disseminations in altered rocks such as listvenites [4,20,24–28].

Mineralogy consists of Ca-Mn-Mg-Fe carbonates, quartz, skarn silicates, magnetite, sulfides, and native elements, which vary from place to place with the style of mineralization depending on the major factor controlling it [27,29]. The most common is the Pb-Zn-Ag mineralization with galena and sphalerite, associated with pyrite and chalcopyrite; arsenopyrite, pyrrhotite, and rare Sb minerals. The main gangue minerals are hydrothermal carbonates (calcite, dolomite, siderite, and rhodochrosite), quartz, and barite. Additionally, rare parageneses such as Cu-Bi-Au-Te with Bi sulfosalts, Bi sulphotellurides, native Au and Bi [15,16,21], Ni-Sb-As with Ni-Fe sulfarsenides and Pb-Sb sulfosalts [20,28,30,31], Sn with stannite group minerals [4], and Ag-Sb with Ag sulfosalts [32] occur.

2.2. Kizhnica-Hajvalia-Badovc Ore Field

The Kizhnica-Hajvalia-Badovc ore field, located in the southern part of the TMB, contains three Pb-Zn-Ag polymetallic deposits (Figure 2), mined in the 20th century: the Hajvalia and Badovc underground mines and the Kizhnica open-pit mine. The oldest rocks in the area belong to the Paleozoic-Triassic metasediments complex, composed of metamorphic schists and marbles. The ultramafic complex (Triassic-Jurassic age) consists of serpentinized peridotites and basalts. The serpentinites near tectonic zones were affected by hydrothermal fluid migration during the main stage of Oligocene-Miocene ore formation in the area, and listvenites were formed as product of ultramafic rocks alteration by hydrothermal fluids [20]. They are composed mainly of Fe-Mn carbonates (siderite-rhodochrosite) and quartz. The Jurassic series with tectonic melanges and olistholites consists of different metamorphic rocks. This series is composed of rocks metamorphosed in the greenschist facies in the east, as well as calcareous schists in the west. Calcareous schists host younger mineralized metasomatic carbonate bodies. The eastern part of the ore field contains flysch series of Jurassic-Cretaceous age. They consist of fining-upward sequences of conglomerates, silty-calcareous units, greywacke, sandy and silty lithologies, and calcareous sandstone to pebble conglomerates with marine and terrestrial contributions [18]. The youngest and most extensive units are Neogene volcanic and volcanoclastic rocks (mainly andesites). Two types of intrusive dikes and sills have been identified in the ore field (hornblende-biotite porphyry andesite and feldspar porphyry andesite). Three NNW-SSE tectonic zones control Pb-Zn mineralization (Hajvalia-Badovc, Kizhnica, and Okosnica) (Figure 2) [33]. Numerous polymetallic mineralization styles including veins, stockwork-impregnation, carbonate-replacement, listvenite-hosted, and skarn or hornfels are observed within the ore field. In addition, three main metallogenic zones can be distinguished: Bi-Cu ± Au in the east, Pb-Zn-Sb in the west, and Sb-As-Tl-Hg in the south (Figure 2).

The Pb-Zn-Ag Kizhnica deposit occurs at the contact (1600 m long × 30 m wide) between serpentinites with a Lower Cretaceous flysch series and is located in close proximity to the volcanic rocks. Irregular ore bodies occur as veins, lenses, and impregnations [4,33]. The hydrothermal mineralization comprises Pb-Zn-Fe-Cu sulfides, Pb-Sb sulfosalts, Fe-Mn-Ca carbonates, and quartz.

The Pb-Zn-Ag Hajvalia deposit is classified as carbonate replacement type and occurs as irregular ore bodies hosted in marbles of the Paleozoic metasedimentary complex, which is composed of phyllite, sericite, and quartz-sericite schists [34]. The hydrothermal mineralization comprises Pb-Zn-Fe-Cu sulfides, magnetite, Pb-Sb sulfosalts, Fe-Mn-Ca carbonates, and quartz.

The Pb-Zn-Ag Badovc deposit, consisting of veins and disseminations, occurs at the contact between altered serpentinites (listvenites) and andesites. Two types of mineralization can be found in Badovc: massive-vein-banded ore and listvenite-hosted disseminated ore. Massive ore consists of Fe-Mn carbonates, quartz, sphalerite, galena, Pb-Sb sulfosalts (boulangerite, semseyite, chovanite, and jamesonite), pyrite, and marcasite [20,35]. Mineralization disseminated in listvenite consists of Fe-Mn carbonates and quartz with sphalerite, galena, pyrite, chalcopyrite, tetrahedrite, sulfarsenides (gersdorffite, Sb-rich gersdorffite, ullmannite, and arsenopyrite), Pb-Sb sulfosalts (boulangerite and semseyite), with minor pyrrhotite, hematite, chromite, native gold, Ni sulfides (millerite and pentlandite), and Ni thiospinels (polydymite and violarite) [20,35]. In addition, younger veins with stibnite, sphalerite, pyrite, berthierite, quartz, and rhodochrosite are observed.

The Janjevo Cu-Bi-Ag(Pb,W) occurrence is located in the southeastern part of the ore field (Figure 2) [36,37]. The contact metasomatic-type mineralization occurs on the contact of the flysch series and andesites and consists of siderite, arsenopyrite, chalcopyrite, members of tetrahedrite group minerals, pyrite, and aikinite, with minor galena, sphalerite, löllingite, native Bi, ferberite, quartz, and several sulfosalts (bournonite, cosalite, bismuthinite, krupkaite, gustavite, pearceite, and wittichenite) [37].

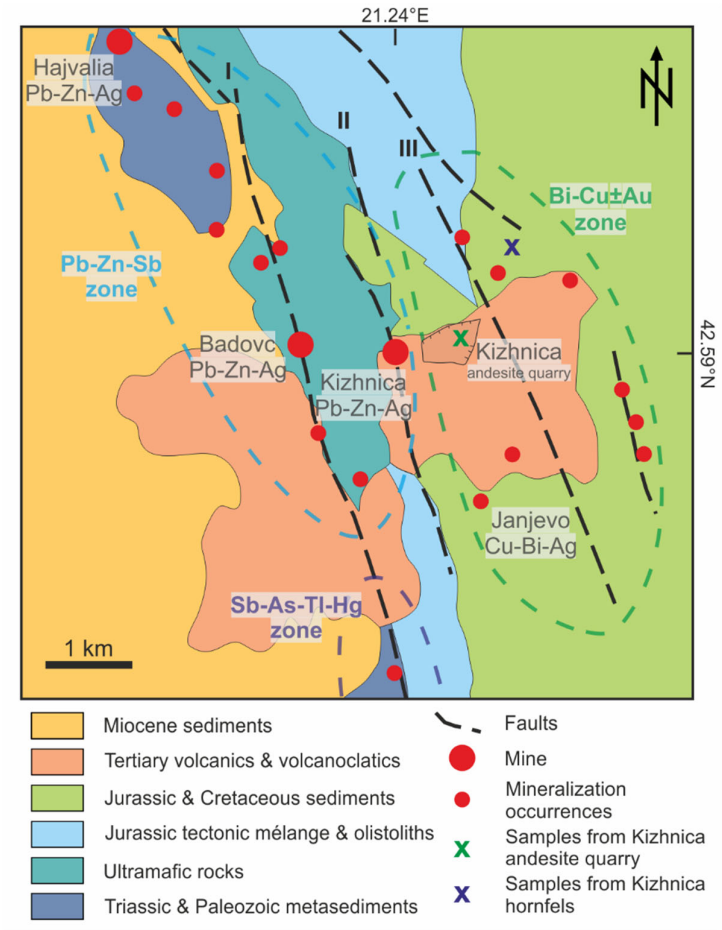

Figure 2. Simplified geological map of the Hajvalia- Kizhnica- Badovc ore field. Abbreviations: I = The Hajvalia-Badovc Tectonic Zone; II = The Kizhnica Tectonic Zone; III = The Okosnica Tectonic Zone.

To the east of the Kizhnica-Hajvalia-Badovc ore field, the Slivovo Au-Ag deposit has been documented [18]. This Au-Ag-Bi-Te mineralization is directly related to the hornblende-biotite porphyry andesite that intersects the calcareous unit and the non-calcareous greywacke unit of the Cretaceous flysch series. In addition, minor hornfels, marble, and pyroxene skarnoid occur at the contact between flysch series units with porphyry. The mineralization consists of pyrite, arsenopyrite, base metal sulfides, bismuthinite, native Au and Bi, tellurides, quartz, and dolomite [18].

3. Samples and Methods

Mineralized rocks samples for mineralogical and geochemical studies were collected from two localities in the eastern part of the Kizhnica ore field. The first locality is the active Kizhnica andesite quarry, which contains veinlets with polymetallic mineralization and one pyrite-galena-quartz brecciated vein (Figure 3a) in the northern part of the quarry. While pyrite and hematite are common, Cu-Bi mineralized samples are rare (Figure 3b,c). Rocks uncovered during the ongoing exploitation in the quarry were sampled systematically during fieldwork from 2016 to 2021 and used for this study. Samples from the second locality were collected to the north of the quarry, where flysch series, locally altered and gossanous, are exposed at the surface. A piece of old drill core from Trepça Mining Company's old prospect drilling works was found at the top of the hill. The drill core, approximately 0.5 m long and with 8 cm diameter, was composed of a distinctive contact rock—hornfels with macroscopically visible disseminated ore miner-

als (Figure 3d–f). Similar hornfelses, at the contacts of flysch series and hornblende-biotite porphyry dikes, are known from drill holes east of Kizhnica, from the Slivovo Au-Ag Project [17].

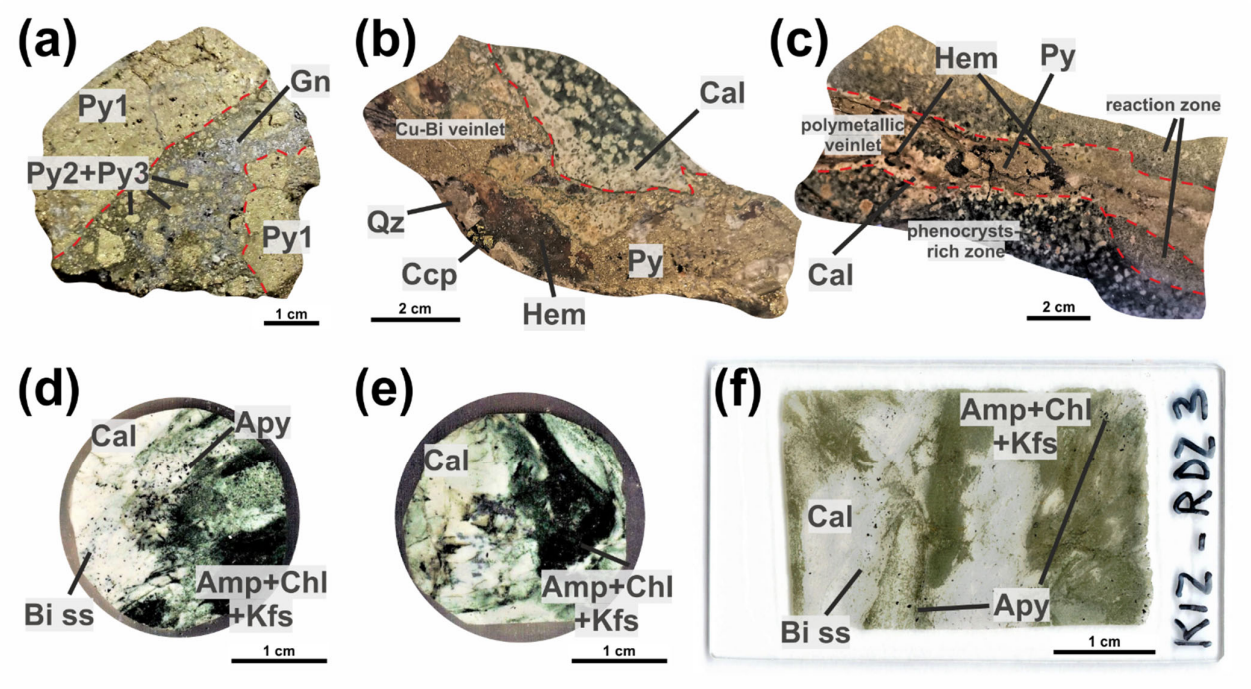

Figure 3. Types of Cu-Bi-Au mineralization from the Kizhnica andesite quarry (**a**–**c**) and Kizhnica hornfels (**d**–**f**): (**a**) pyrite-galena-quartz breccia with 3 types of pyrite and galena; (**b**) Cu-Bi veinlet with pyrite, hematite, chalcopyrite, quartz, and calcite; (**c**) Cu-Bi veinlet with pyrite, hematite, and calcite; phenocrysts-rich zone and reaction zone in andesite; (**d**) hornfels composed of amphiboles, chlorites, K-feldspar with mineralized calcite with idiomorphic arsenopyrite crystals, and bismuth sulfosalts; (**e**) hornfels composed of amphiboles, chlorites, K-feldspar with calcite; (**f**) hornfels composed of amphiboles, chlorites, and K-feldspar with mineralized calcite. Abbreviations: Apy = arsenopyrite; Amp = amphiboles; Bi ss = bismuth sulfosalts; Cal = calcite; Ccp = chalcopyrite; Chl = chlorites; Gn = galena; Hem = hematite; Kfs = K-feldspar; Qz = quartz; Py = pyrite.

Samples from each locality were examined macroscopically, and 15 thin and polished sections were prepared for mineralogical studies. Mineral assemblages and textural relationships were studied using reflected and transmitted light microscopy. The quantitative element composition of sulfides and sulfosalts was obtained in eight samples representing major types of mineralization using electron probe microanalysis (EPMA). Trace element composition of selected minerals (pyrite, chalcopyrite, arsenopyrite, tetrahedrite, and sphalerite) was determined by laser ablation inductively coupled plasma mass spectrometry (LA-ICP-MS) in three samples.

Ore minerals were analyzed using a JEOL Super Probe 8230 in the Laboratory of Critical Elements at Faculty of Geology, Geophysics and Environmental Protection, AGH-UST, Kraków Poland. The following operating conditions and standards were used: accelerating voltage 20 kV, beam current 20 nA, and a beam diameter up to 5 μm. The following X-ray emission lines were used: SK_α; FeK_α; CuK_α; ZnK_α (TGM); AsL_α; SbL_α; AgL_α (without sulfarsenides); SeL_α and TeL_α (tetradymite and native Au); BiM_α; PbM_α (tetradymite, native Au, and Bi-sulfosalts); HgM_α (TGM and native Au); AuM_α (native Au); NiK_α and CoK_α (sulfarsenides). The detection limits for analyzed elements are shown in Table S1. Natural mineral standards (ZnS, PbS, FeS_2, and Sb_2S_3) and synthetic compounds (Bi, Ag Ni, Co, Au, Se, PbTe, HgTe, $CuFeS_2$, and GaAs) were used for calibration. Interferences between the element emission lines were calculated using autocorrections based on the standard materials. Microprobe microanalyses were conducted for

the determination of iron, copper, and zinc contents used as internal standards during LA-ICP-MS analyses for pyrite (Fe), chalcopyrite (Fe), arsenopyrite (Fe), tetrahedrite (Cu), and sphalerite (Zn).

Trace element concentrations in pyrite, chalcopyrite, arsenopyrite, tetrahedrite, and sphalerite were measured using a PerkinElmer ELAN DRC-e ICP mass spectrometer combined with a New Wave UP193-FX excimer laser ablation system at the Geological Institute, Bulgarian Academy of Sciences, Sofia, Bulgaria. The ablation was conducted in He medium. To maximize sensitivity, the ICP-MS was optimized daily concerning the oxide production rate of ThO/Th (0.5%). Operating conditions of the laser system include 6 Hz repetition rate; 20 to 35 μm spot size; and energy density on analyzed minerals and standards of 3.3–3.4 J/cm^2 (at 35 μm spot) and 2.9–3.1. J/cm^2 (at 20 and 25 μm m spot). The nebulizer gas flow rate was 0.8 L/min, while auxiliary and make-up gas flows rates were 0.92 L/min. The analysis time was 100 s (background: 40 s, laser-on the sample: 60 s). The acquisition dwells time was set to 0.02 s for ^{71}Ga, ^{74}Ge, ^{107}Ag, ^{125}Te, ^{202}Hg, ^{205}Tl; to 0.03 s for ^{115}In, ^{118}Sn; to 0.04 s for ^{197}Au; and 0.01 s for all other monitored isotope masses—^{34}S, ^{49}Ti, ^{51}V, ^{53}Cr, ^{55}Mn, ^{57}Fe, ^{59}Co, ^{60}Ni, ^{65}Cu, ^{66}Zn, ^{75}As, ^{77}Se, ^{82}Se, ^{95}Mo, ^{111}Cd, ^{121}Sb, ^{181}Ta,^{182}W, ^{208}Pb, and ^{209}Bi. The targeted areas in the polished sections were predefined to avoid mineral inclusions. Repeated external standardization was conducted by analyzing NIST SRM 610 glass standard and the USGS Mass 1 sulfide standard.

Data reduction was done using SILLS software [38]. During data reduction, peak-shaped fluctuations of the intensity signal of some isotopes were investigated to exclude the influence of other minerals on the chemical composition of the studied minerals. Limits of detection for each isotope mass are determined for every analysis and may differ.

4. Results

4.1. Kizhnica Quarry

Mineralization forms steep vertical veins with a N-S strike, which can be observed in walls of the Kizhnica andesite quarry. Plagioclase phenocrysts, as well as euhedral Ca-amphiboles, occur in the andesite contacts with pyrite- and hematite-rich veinlets. Pyrite occurs usually in a form of disseminated crystals in altered andesite or as veinlets and veins with quartz and calcite. Hematite forms veinlets of coarse crystalline aggregates (specularite). Generally, two types of mineralized veins/veinlets are observed: (1) Cu-Bi veinlets and (2) pyrite-galena-quartz brecciated vein. Copper-bismuth veinlets are composed of pyrite, hematite, calcite, quartz, chalcopyrite, epidote/Ca amphiboles with minor Bi sulfosalts and tetrahedrite group minerals (TGM) (Figures 3b,c; 4a–d). Copper-Bi veinlets reach a length of up to 10 cm. Additionally, greenish secondary copper minerals are present here. The second type of Bi-Cu mineralization occurs within the galena-quartz vein, where strong brecciation is observed (Figure 3a). Pyrite-galena-quartz brecciated vein contains also sphalerite, Bi sulfosalts, TGM, marcasite, covellite, calcite, and baryte (Figure 4e–i). The mineralized zone is about 30 cm thick and a few meters long.

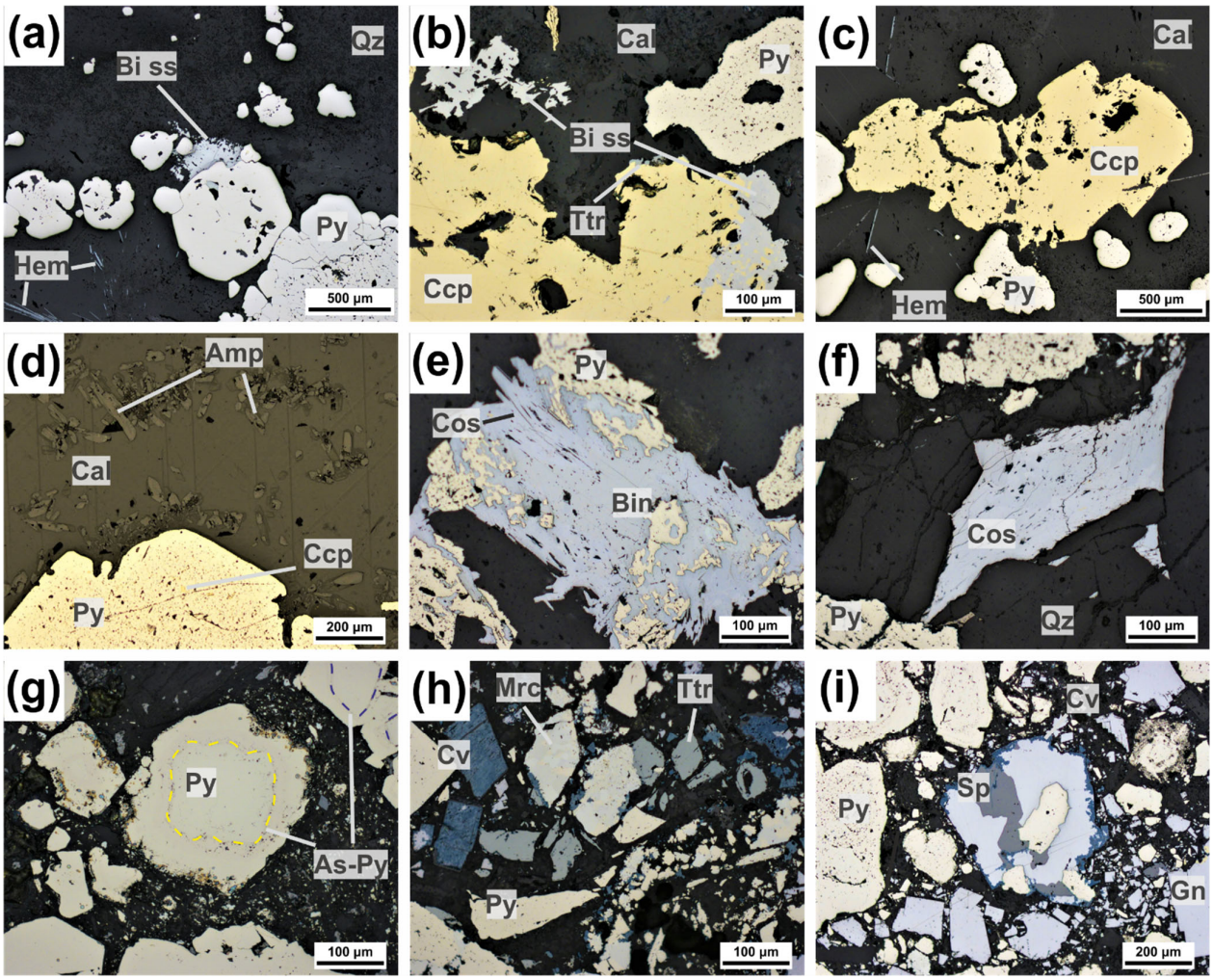

Figure 4. Reflected-light photomicrographs of polymetallic mineralization from the Kizhnica quarry: (**a**) aggregates of Bi sulfosalts overgrowing pyrite; hematite crystals in quartz; (**b**) aggregates of Bi sulfosalts and tetrahedrite group minerals overgrowing chalcopyrite in calcite veinlet; (**c**) subhedral chalcopyrite crystal, pyrite, and hematite crystals in calcite veinlets; (**d**) pyrite crystal with chalcopyrite inclusions in calcite veinlet with euhedral amphibole crystals; (**e**) aggregate of cosalite with bismuthinite replacing pyrite; (**f**) cosalite crystals in quartz–pyrite matrix; (**g**) irregular pyrite with arsenian pyrite zones from pyrite-galena-quartz breccia; (**h**) pyrite, tetrahedrite group minerals, marcasite, and covellite clasts from pyrite-galena-quartz breccia; (**i**) Pyrite crystals and galena–sphalerite aggregates with secondary covellite from pyrite-galena-quartz breccia. Abbreviations: Amp = amphiboles; As-Py = arsenian pyrite; Bi ss = bismuth sulfosalts; Bin = bismuthinite; Cal = calcite; Ccp = chalcopyrite; Cos = cosalite; Cov = covellite; Gn = galena; Hem = hematite; Mrc = marcasite; Qz = quartz; Py = pyrite; Sp = sphalerite; Ttr = tetrahedrite group minerals.

4.1.1. Bismuth Sulfosalts

Bismuthinite-Aikinite Series

Sulfosalts of the bismuthinite-aikinite series are rare in the studied samples. Three basic members of this series: bismuthinite, krupkaite, and aikinite were identified. Precise identification was based on a calculation of the degree of aikinite substitution (n_{aik}) ($Bi^{3+} + \square \leftrightarrow Pb^{2+} + Cu^{+}$) proposed by Topa et al. [39]. The value of n_{aik} was calculated following the scheme $n_{aik} = 25(x + y)/2$, where x is the number of Cu atoms and y the number of Pb atoms in the formulae, based on the sum Ag + Bi + Sb + Fe + As + (Pb + Cu)/2 = 8 atoms.

Bismuthinite was found in pyrite-galena-quartz brecciated vein as elongated crystals up to 300 µm in size and is spatially associated with other Bi phases (cosalite and krupkaite) forming the center of grains overgrown/replaced by them in quartz matrix or

older corroded pyrite aggregates (Figure 4e; Figure 5a,b). The degree of aikinite type substitution (n_{aik}) in bismuthinite from Kizhnica ranges from 2.22–11.08 (Table 1; Figure 6). It contains minor Fe (up to 1.32 wt.%). The empirical formula for studied bismuthinite was calculated on the basis of the sum Ag + Bi + Sb + Fe + As + (Pb + Cu)/2 = 8 atoms and can be expressed as $(Bi_{7.14–7.90}Pb_{0.08–0.42}Cu_{0.09–0.44}Fe_{0.00–0.45}As_{0.00–0.04}Sb_{0.01–0.03})_{\Sigma 8.09-8.43}S_{11.23-12.01}$. Obtained results fit the intervals confirmed by crystallographic studies given by Topa et al. [39] and are not over-substituted as it was reported in many world localities [40].

Krupkaite is rare and forms intergrowths with aikinite (Figure 5c) or irregular aggregates forming reaction zones between bismuthinite and cosalite (Figure 5b) in pyrite-galena-quartz vein. The size of the krupkaite aggregates is up to 10 μm. The degree of aikinite type substitution (n_{aik}) in krupkaite is 46.51–48.65 (Table 1; Figure 6). The chemical composition of krupkaite corresponds to the ideal krupkaite stoichiometry. It contains only up to 0.27 wt.% Sb. The formula of krupkaite can be expressed as $(Cu_{1.85-1.93}Pb_{1.82-1.94}Bi_{6.05-6.14}Sb_{0.01-0.04})_{\Sigma 9.83-9.94}S_{11.56-11.94}$. A similar form, position, and chemical composition of krupkaite within the Trepça Mineral Belt was observed in the Bi-Au-Cu ore from Mazhiq [19,21].

Aikinite forms irregular intergrowths with krupkaite up to 150 μm in size (Figures 4c; 5c) in Cu-Bi veinlets. The empirical formula for studied akinite can be expressed as $(Cu_{3.25–3.82}Pb_{3.17–3.71}Fe_{0.00–0.05}Bi_{4.20–4.76}Sb_{0.01–0.02})_{\Sigma 11.21–11.75}S_{11.33–11.70}$, while the degree of aikinite type substitution is 84.07–96.66 (Table 1; Figure 6).

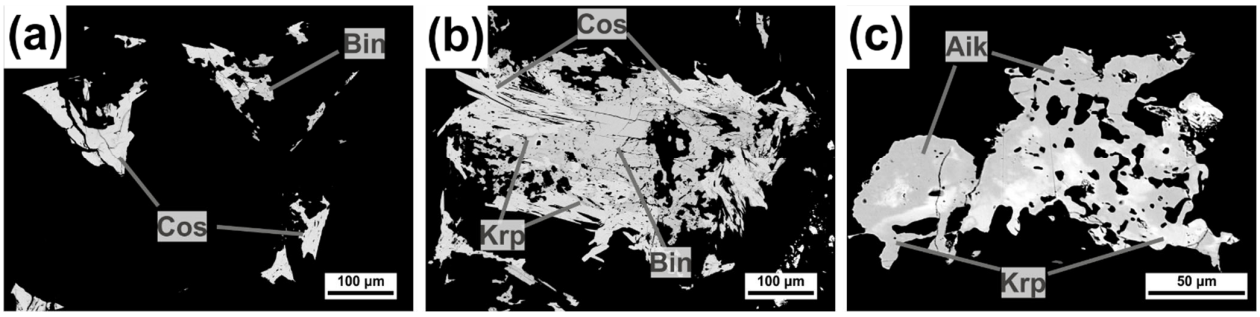

Figure 5. Back-scattered electron (BSE) images showing Bi sulfosalts from the Kizhnica quarry: (**a**) cosalite and bismuthinite crystals; (**b**) aggregate of cosalite and bismuthinite with krupkaite zones between them; (**c**) aikinite–krupkaite aggregate. Abbreviations: Aik = aikinite; Bin = bismuthinite; Cos = cosalite; Krp = krupkaite.

Table 1. Representative EPMA data for members of bismuthinite-aikinite series: bismuthinite [1,2], krupkaite [3,4], and aikinite [5–8] from Kizhnica quarry. The empirical formula was calculated based on the sum Ag + Bi + Sb + Fe + As + (Pb + Cu)/2 = 8 atoms, b.d.l. = below detection limit.

Analyses	wt.%									apfu								Cations	n_{aik}
	S	Fe	Cu	Ag	Sb	Pb	As	Bi	Total	S	Fe	Cu	Ag	Sb	Pb	As	Bi		
1	**19.09**	b.d.l.	0.30	b.d.l.	0.08	0.81	b.d.l.	81.85	102.14	12.01	-	0.09	-	0.01	0.08	-	7.90	8.09	2.22
2	18.94	0.45	1.10	b.d.l.	0.06	3.58	b.d.l.	78.85	102.99	11.72	0.16	0.34	-	0.01	0.34	-	7.49	8.34	8.78
3	17.97	b.d.l.	5.54	b.d.l.	0.23	17.93	b.d.l.	59.89	101.58	11.94	-	1.86	-	0.04	1.84	-	6.10	9.85	46.51
4	17.74	b.d.l.	5.69	b.d.l.	0.08	18.65	b.d.l.	58.60	100.76	11.94	-	1.93	-	0.01	1.94	-	6.05	9.94	48.65
5	16.92	0.14	10.57	b.d.l.	b.d.l.	32.57	b.d.l.	42.35	102.58	11.50	0.05	3.62	-	-	3.42	-	4.42	11.52	91.95
6	16.81	0.06	10.60	b.d.l.	b.d.l.	34.47	b.d.l.	40.51	102.48	11.59	0.03	3.69	-	-	3.68	-	4.29	11.68	95.30
7	16.91	0.11	10.94	b.d.l.	b.d.l.	34.44	b.d.l.	39.57	102.01	11.70	0.04	3.82	-	-	3.69	-	4.20	11.75	96.19
8	16.74	b.d.l.	10.78	b.d.l.	0.12	34.57	b.d.l.	39.78	101.99	11.61	-	3.77	-	0.02	3.71	-	4.23	11.74	96.66

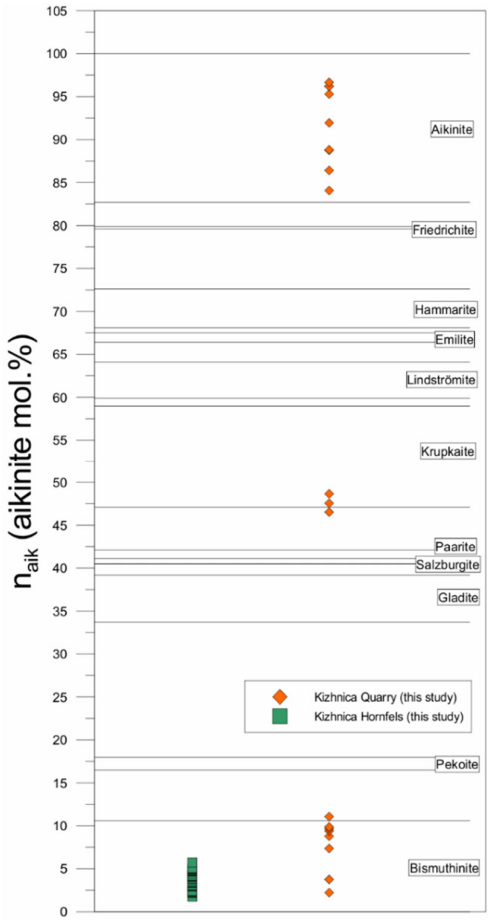

Figure 6. Position of the species of the bismuthinite-aikinite series from the Kizhnica area determined by their n_{aik} after [38].

Cosalite

Cosalite occurs as intergrowths with bismuthinite and krupkaite in quartz matrix or older corroded pyrite aggregates in pyrite-galena-quartz vein (Figure 4a,b,e,f). It forms crystals up to 300 μm long. Small chalcopyrite and tetrahedrite inclusions up to a few μm occur within cosalite crystals. The empirical formula for studied cosalite based on 20 anions [41] can be expressed as $(Cu_{0.87–1.33}Ag_{0.19–0.38})_{\Sigma 1.06–1.63}(Pb_{6.93–7.45}Fe_{0.00–0.27})_{\Sigma 6.93–7.63}(Bi_{7.57–8.19}Sb_{0.08–0.21})_{\Sigma 7.73–8.28}S_{\Sigma 20}$ (Table 2). Following the general formula for cosalite $(Cu_xAg_{i+s}Pb_{8–2s–0.5(x+i)}Bi_{8+s}S_{20})$ proposed by Topa and Makovicky [41], cosalite from Kizhnica is characterized by mainly 2(Cu + Ag) ↔ Pb substitution, where parameter x (the content of Cu) is in the range from 0.87 up to 1.33. Silver is partially involved in substitution with Cu, and parameter i is in the range from 0.01 up to 0.38. Additionally, substitution Ag + Bi ↔ 2Pb (lillianite type of substitution) is presented in a low degree—the content of silver (s) is in the range from 0.02 up to 0.26 apfu. Content of trivalent elements (Bi + Sb + As) is close to the ideal number 8 apfu (in the range 7.73–8.28), showing limited substitution of Ag for Bi. The Sb ↔ Bi substitution is not significant—the content of Sb is up to 0.6 wt.% in cosalite from the quarry. Generally, Sb could substitute in higher degree into the cosalite structure as it was documented at many localities, e.g., Stan Terg [16], as well as Hviezda, Slovakia [40]. Following the known substitutions in cosalite (Figures 7 and 8a–c) [11,13,16,19,21,41–43] samples from the Kizhnica quarry are similar to the samples from epithermal Au-Bi-Cu or skarn Cu deposits in Romania (Ocna de Fier) [40] or Mazhiq (Trepça Mineral Belt) [18,20], but they are distinct from the skarn known in the Serbo-Macedonian metallogenic province (Rudnik, Kram, Stan Terg) [11,16,42].

Table 2. Representative EPMA data for cosalite from the Kizhnica quarry. The empirical formula was calculated based on the 20 anions, b.d.l. = below detection limit.

Analyses	wt.%									apfu								Cations
	S	Fe	Cu	Ag	Sb	Pb	As	Bi	Total	S	Fe	Cu	Ag	Sb	Pb	As	Bi	
1	16.76	b.d.l.	1.73	0.77	0.43	38.58	b.d.l.	41.65	99.93	20.00	-	1.04	0.27	0.13	7.12	-	7.62	16.21
2	16.72	0.07	1.79	0.77	0.27	38.34	b.d.l.	43.17	101.13	20.00	0.05	1.08	0.27	0.09	7.10	-	7.92	16.50
3	16.66	b.d.l.	1.43	0.55	0.57	39.23	b.d.l.	42.93	101.39	20.00	-	0.87	0.19	0.18	7.29	-	7.90	16.44
4	16.63	b.d.l.	1.81	0.69	0.32	38.27	b.d.l.	43.11	100.84	20.00	-	1.10	0.25	0.10	7.12	-	7.95	16.52
5	16.56	b.d.l.	1.53	0.74	0.67	38.93	b.d.l.	41.52	99.99	20.00	-	0.93	0.27	0.21	7.28	-	7.69	16.39
6	16.53	0.05	1.45	0.75	0.47	38.48	b.d.l.	43.46	101.19	20.00	0.04	0.88	0.27	0.15	7.20	-	8.07	16.60
7	16.52	b.d.l.	1.91	0.72	0.56	38.65	b.d.l.	40.74	99.11	20.00	-	1.16	0.26	0.18	7.24	-	7.57	16.43
8	16.49	0.05	1.79	0.83	0.26	39.20	b.d.l.	41.08	99.70	20.00	0.03	1.09	0.30	0.08	7.36	-	7.65	16.52
9	16.45	b.d.l.	1.71	0.78	0.25	39.12	b.d.l.	41.28	99.61	20.00	-	1.05	0.28	0.08	7.36	-	7.70	16.47
10	16.31	b.d.l.	2.16	0.83	0.48	39.26	b.d.l.	40.52	99.56	20.00	-	1.33	0.30	0.15	7.45	-	7.62	16.87
11	16.31	b.d.l.	1.95	0.86	0.44	38.95	b.d.l.	40.89	99.45	20.00	-	1.20	0.31	0.14	7.39	-	7.69	16.77
12	16.26	0.18	1.65	0.75	0.28	37.80	b.d.l.	43.41	100.32	20.00	0.13	1.03	0.27	0.09	7.19	-	8.19	16.90

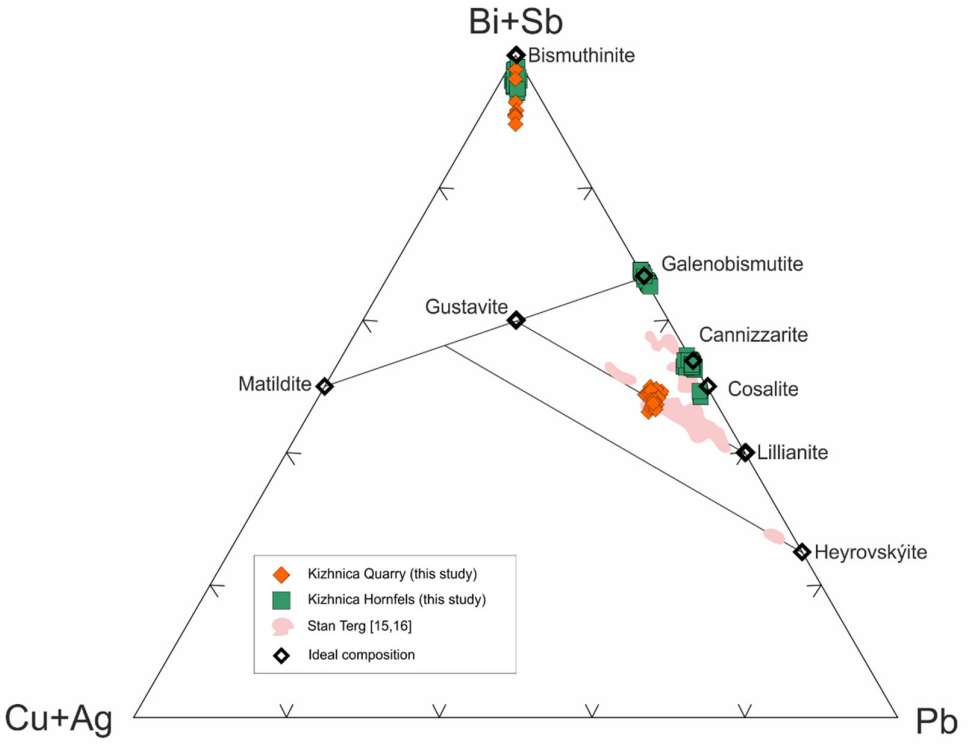

Figure 7. Ternary plot Cu + Ag vs Bi + Sb vs Pb of bismuth sulfosalts from the Kizhnica area and the Stan Terg deposit [15,16].

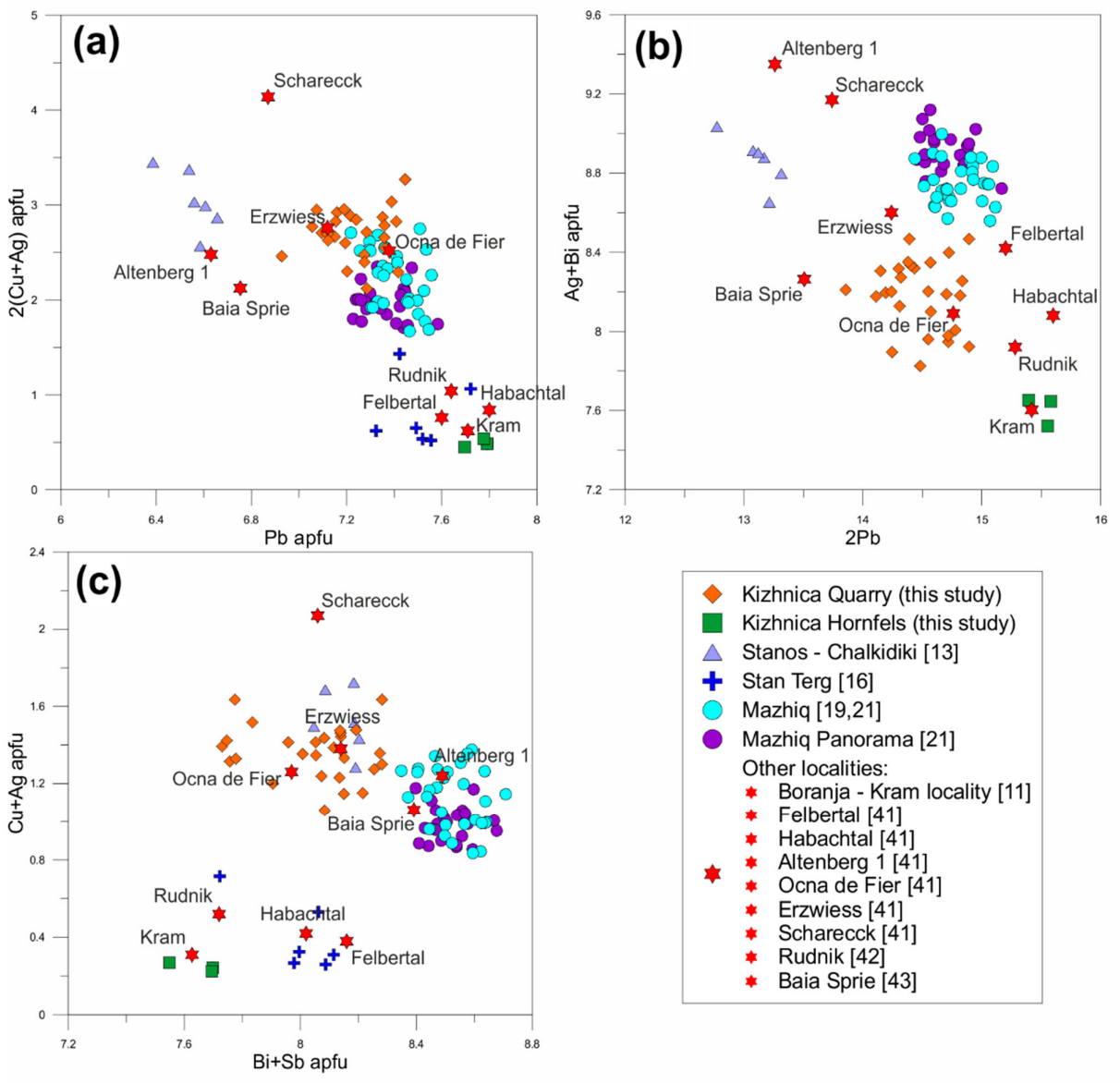

Figure 8. Binary plots showing the chemical composition of cosalite from the Kizhnica area and known locations of cosalite from the literature [11,13,15,16,19,21,41–43]: (**a**) 2(Cu + Ag)vs Pb (apfu); (**b**) Ag + Bi vs 2Pb (apfu); (**c**) Cu + Ag vs Bi + Sb (apfu).

4.1.2. Pyrite

Pyrite is the most widespread ore mineral in the Kizhnica andesite quarry. It forms disseminated euhedral or subhedral crystals up to 2 cm in size, and irregular veinlets in andesite (Figures 3a–c; 4a–i). It is the major component of both Cu-Bi veinlets, and pyrite-galena-quartz brecciated vein. Numerous tiny inclusions of chalcopyrite (Figure 4d), galena, Bi sulfosalts (Figure 9a), and Ti oxides can be observed in pyrite crystals. Based on textural relationships and chemical composition, three main pyrite types can be distinguished. The LA-ICP-MS analyses of pyrite are shown in Table 3.

Pyrite 1 (Py1) occurs as disseminated crystals and veinlets in andesite. Larger crystals from Cu-Bi veinlets were analyzed by LA-ICP-MS (Table 3). Pyrite 1 is characterized by the highest Co content (up to 121 ppm), while As content is variable (740–10130 ppm). Generally, all the LA-ICP-MS spectra are relatively flat (Figure 10b), only cobalt shows small variations with noticeable enrichment in outer zones (Figures 9a; 10a).

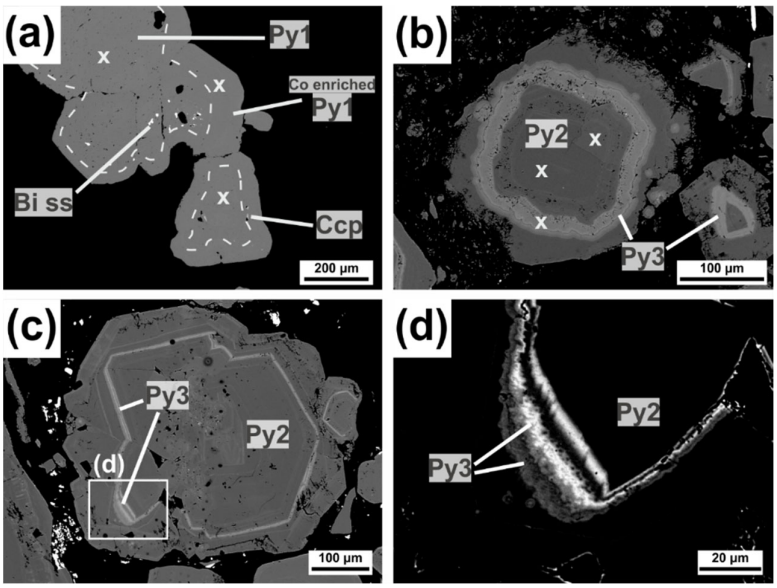

Figure 9. Back-scattered electron (BSE) images showing different types of pyrite from the Kizhnica quarry: (**a**) pyrite 1 (Py1) containing inclusions of bismuth sulfosalts and chalcopyrite, outer rim enriched in Co; (**b**) pyrite 2 (Py2) with a zone of arsenian pyrite 3 (Py3); (**c**) pyrite 2 (Py2) with arsenian pyrite 3 (Py3) zones; (**d**) detail of image (**c**) irregular zones of arsenian pyrite (Py3) in pyrite 2 (Py2). Abbreviations: Bi ss = bismuth sulfosalts; Ccp = chalcopyrite; Py = pyrite; x = LA-ICP-MS spots.

Table 3. LA-ICP-MS analyses of pyrite from Kizhnica quarry. Values are in ppm, Fe in wt. % (microprobe).

Mineralization	Hydrothermal Veinlets														
Type	Veinlets (n = 5); Py1					Disseminated (n = 8); Py2					Disseminated (n = 6); Py3				
Element	MIN	MAX	ST DEV	AVG	$n_{a.d.l.}$	MIN	MAX	ST DEV	AVG	$n_{a.d.l.}$	MIN	MAX	ST DEV	AVG	$n_{a.d.l.}$
Ti	15	24	3.70	18	5	10	29	6.36	19	8	18	38	9.24	25	4
V	0.66	0.66	n.c.	n.c.	1	2.57	3.01	0.31	2.79	2	5.90	5.90	n.c.	n.c.	1
Cr	34	51	6.04	41	5	30	44	5.50	36	8	23	41	6.06	33	6
Mn	52	56	2.13	54	5	45	295	87	87	8	44	57	4.52	48	6
Fe	46.25	46.80	0.23	46.65	5	46.12	46.76	0.23	46.42	8	44.29	46.91	0.97	46.22	6
Co	5.26	121	52	49	5	3.73	24	6.88	12	7	0.96	7.91	2.89	3.57	6
Ni	8.62	8.62	n.c.	n.c.	1	3.39	17	8.25	8.29	3	6.83	6.83	n.c.	n.c.	1
Cu	2.57	3.77	0.85	3.17	2	2.48	7.36	2.67	5.54	3	5.53	130	71	48	3
Zn	5.84	7.08	0.87	6.46	2	8.70	11	1.95	10	3	7.25	11	2.74	9.18	2
Ga	b.d.l.	b.d.l.	n.c.	n.c.	0	20	20	n.c.	n.c.	1	1.46	1.46	n.c.	n.c.	1
Ge	b.d.l.	b.d.l.	n.c.	n.c.	0	1.43	2.57	0.63	1.84	3	4.80	4.80	n.c.	n.c.	1
As	743	10131	3831	3501	5	235	1298	366	672	8	1215	49609	19406	10018	6
Se	4.79	6.19	0.99	5.49	2	9.54	9.54	n.c.	n.c.	1	b.d.l.	b.d.l.	n.c.	n.c.	0
Mo	b.d.l.	b.d.l.	n.c.	n.c.	0	1.39	1.39	n.c.	n.c.	1	6.47	6.47	n.c.	n.c.	1
Ag	b.d.l.	b.d.l.	n.c.	n.c.	0	0.20	0.25	0.03	0.23	2	3.11	3.11	n.c.	n.c.	1
In	0.24	0.24	n.c.	n.c.	1	0.06	0.06	n.c.	n.c.	1	0.34	0.34	n.c.	n.c.	1
Sn	b.d.l.	b.d.l.	n.c.	n.c.	0	b.d.l.	b.d.l.	n.c.	n.c.	0	8.66	8.66	n.c.	n.c.	1
Sb	b.d.l.	b.d.l.	n.c.	n.c.	0	b.d.l.	b.d.l.	n.c.	n.c.	0	0.35	1298	645	330	4
Te	b.d.l.	b.d.l.	n.c.	n.c.	0	2.10	2.10	n.c.	n.c.	1	3.34	3.34	n.c.	n.c.	1
W	b.d.l.	b.d.l.	n.c.	n.c.	0	0.54	74	52	37	2	0.97	0.97	n.c.	n.c.	1
Au	0.19	0.79	0.42	0.49	2	0.55	0.55	n.c.	n.c.	1	0.70	2.06	0.73	1.53	3
Hg	b.d.l.	b.d.l.	n.c.	n.c.	0	0.44	0.44	n.c.	n.c.	1	178	178	n.c.	n.c.	1
Tl	b.d.l.	b.d.l.	n.c.	n.c.	0	8.60	8.60	n.c.	n.c.	1	1022	1022	n.c.	n.c.	1
Pb	0.76	0.76	n.c.	n.c.	1	0.30	2.89	1.03	1.29	5	0.70	1794	724	317	6
Bi	0.11	0.70	0.30	0.37	3	0.20	19.52	6.95	4.27	7	0.51	8.67	2.92	3.46	6

Cd and Ta are below minimum detection limit. AVG = average value; b.d.l. = below detection limit; MIN = minimum value; MAX = maximum value; n = number of analyses; $n_{a.d.l.}$ = number of analyses above detection limit; n.c. = not calculated; STDEV = standard deviation.

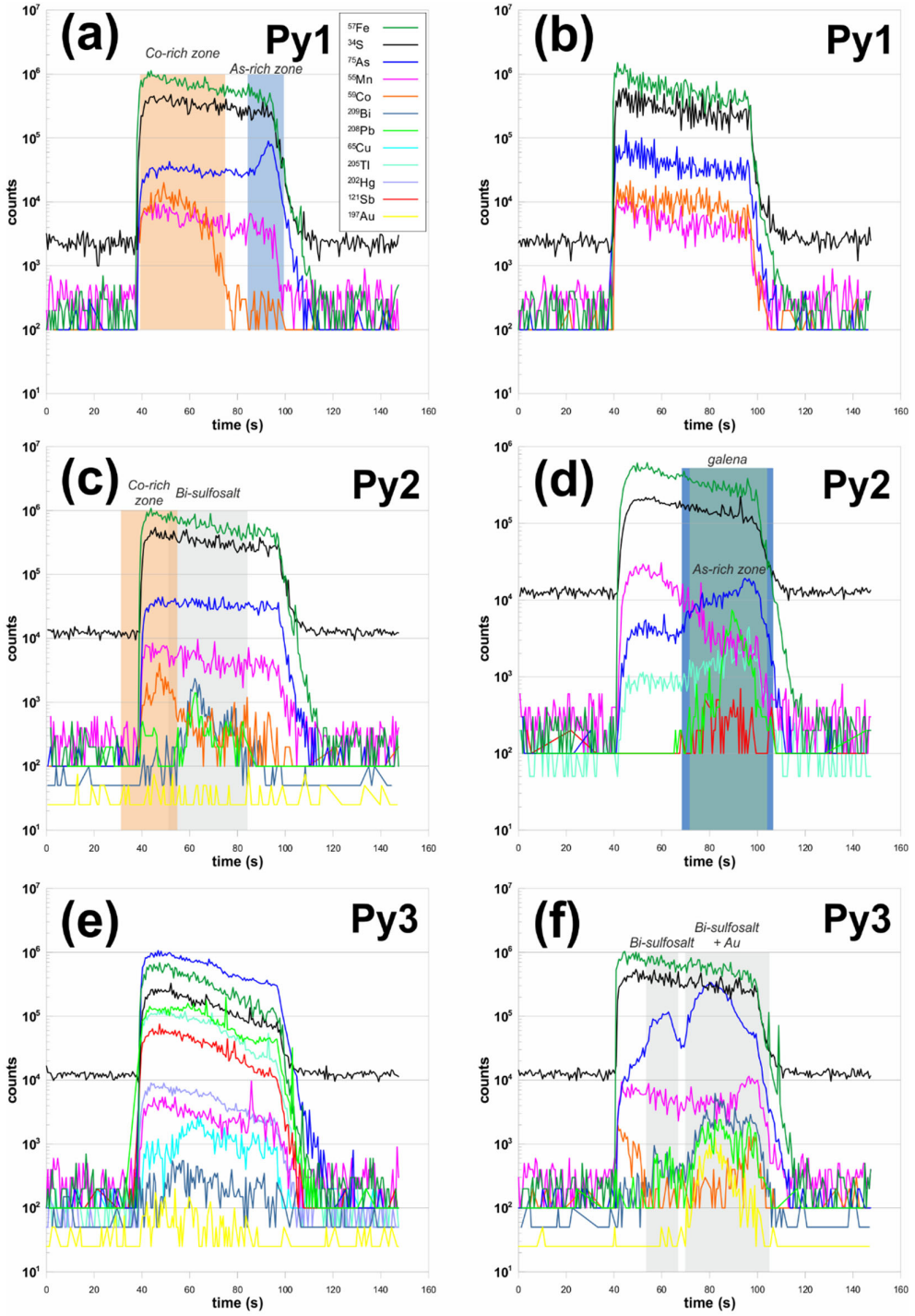

Figure 10. Representative time-resolved laser ablation ICP-MS depth profiles of pyrite, Co, and As-rich zones (highlighted in orange) in pyrite (highlighted in blue) and associated inclusions (highlighted in gray and green) from the Kizhnica quarry. (**a**) Spectra of pyrite 1 with Co and As-rich zone; (**b**) flat spectra of pyrite 1; (**c**) spectra of Py2 with Co-rich zone, the distribution patterns of Bi and Pb could be related to inclusions of Bi-Pb sulfosalt; (**d**) spectra of pyrite 2 enriched in As and Tl, while Pb and Sb are related to galena inclusion and As-rich zone; (**e**) relatively flat spectra of pyrite 3, and the similarly curved distribution patterns of Bi and Cu could be related to inclusions of Bi-Cu sulfosalt; (**f**) spectra of Py3 with variable As content, and the spiky patterns of Bi, Pb, and Au could suggest the occurrence of Bi-Pb inclusions with possible gold.

Py2 and Py3 are observed as subhedral or anhedral rounded crystals within the pyrite-galena-quartz brecciated vein. The younger As-rich pyrite (Py3) crystallized around the Py2 aggregates, forming irregular zonations of varying thicknesses (Figure 9b-d). In addition, small zones enriched in As are observed in this type of pyrite. These zones show higher porosity and the presence of inclusions of other phases. Py2 has the lowest As content (up to 1298 ppm) and the highest Ni content (up to 17 ppm). Some trace elements are likely associated with the presence of inclusions: Bi (up to 20 ppm), Tl (up to 8.6 ppm), Pb (up to 2.89 ppm), Au (up to 0.55 ppm), and Ag (up to 0.25 ppm) (Table 3). LA-ICP-MS spectra of Py2 reveal fluctuations in As and Co content, as well as the presence of galena (Figure 10d) and Bi-Pb sulfosalt inclusions (probably cosalite) (Figure 10c). One measurement showed elevated Tl (~9 ppm), with the Tl spectra showing a correlation with As and no relationship with Sb and Pb, which are associated with galena inclusions (Figure 10d). The lack of Tl and Sb relation in Py2 seems particularly interesting, especially since $2Fe^{2+} \leftrightarrow Tl^{+} + Sb^{3+}$ substitution is reported in (Tl,Sb,As)-rich pyrites from the ore deposits of the southern Apuan Alps (Tuscany, Italy) [44]. On the other hand, a close relationship between Tl and Sb is observed in pyrite 3 (Py3).

Pyrite 3 is especially enriched in As (up to 49,609 ppm) and Au (up to 2.06 ppm) in comparison with pyrite 1 and 2. In addition, higher concentrations of Pb (up to 1794 ppm), Sb (up to 1298 ppm), Tl (up to 1022 ppm), Hg (up to 178 ppm), Cu (up to 130 ppm), Bi (up to 8.67 ppm), and Ag (up to 3.11 ppm) are observed (Table 3). BSE images show that the zones composed of Py3 exhibit oscillatory zonality as well as relatively high porosity with possible nanoinclusions (Figure 9b–d). In addition, Py3 zones are usually too narrow compared to the LA-ICP-MS spot diameter (25/35 μm) to be completely isolated from Py2. Only one analytical point was able to fit entirely into the Py3 zone (Figure 9b; 10e). The distribution pattern of individual elements such as S, Fe, As, Sb, Pb, Tl, Mn, or Hg in Figure 10e is consistent and is associated with the Py3 structure. On the other hand, Cu and Bi spectra suggest their presence as Bi sulfosalt nanoinclusions or inclusions that are probably related to Au enrichment (Figure 10e,f). Ciobanu et al. [45] described elevated contents of Au in aikinite (up to 542 ppm), rather than in bismuthinite (up to 2 ppm) when comparing bismuth chalcogenides in epithermal, skarn, intrusion-related, and orogenic gold systems. In addition, Ciobanu et al. [45] also noted elevated Au content in the cosalite (up to 574 ppm). In Kizhnica, cosalite occurs as inclusions in one of the measured Py3 spots (Figure 10f). LA-ICP-MS measurements showed that not all arsenic-rich zones exhibit elevated Tl, Sb, and Hg contents (Figure 10f). The zones were narrow in the context of LA-ICP-MS analyses, whereas several microprobe analyses could be performed. The formula of Py3 can be expressed as $(Fe_{0.99}Sb_{0.003}Tl_{0.003}Pb_{0.003}Hg_{0.001})_{\sum 1}(S_{1.95–1.96}As_{0.09–0.12})_{\sum 2.04–2.08}$. The presence of Tl, Sb, Pb, and Hg in Py3 is related to the migration of younger low-temperature fluids. The occurrence of mineralization associated with Tl-Sb-As-rich fluids is known from the south-western part of the ore field, within the Triassic marbles, on the southern continuation of the Hajvalia-Badovc tectonic zone (Figure 2). The presence of As-Tl-Sb-rich fluids in the eastern part of the ore field, and especially in proximity to the Cu-Bi-Au zone (Figure 2), suggests a deeper source of these metals, as well as a wider extent of this zone.

4.1.3. Chalcopyrite

Chalcopyrite occurs in Cu-Bi veinlets and forms euhedral or subhedral crystals up to 2 cm in size in association with pyrite, tetrahedrite, and Bi-sulfosalts (Figure 4b,c), as well as tiny inclusions in pyrite (Figure 4d). Additionally, galena-sphalerite-chalcopyrite aggregates are observed in pyrite-galena-quartz vein. Representative LA-ICP-MS analyses of chalcopyrite are shown in Table S2. Chalcopyrite from the Kizhnica quarry is characterized by homogeneous chemical composition, and LA-ICP-MS spectra are relatively flat (Figure 11a,b). The highest variation can be observed in Zn concentrations (117–360 ppm). Other detected trace elements are In (up to 29 ppm), Mn (up to 31 ppm), Ti (up to 24 ppm), and Bi (up to 7 ppm). Bismuth enrichment could be related to tiny Bi-sulfosalts inclusions. Much bigger tetrahedrite group minerals inclusions are also observed in some LA-ICP-MS spectra (Figure 11b).

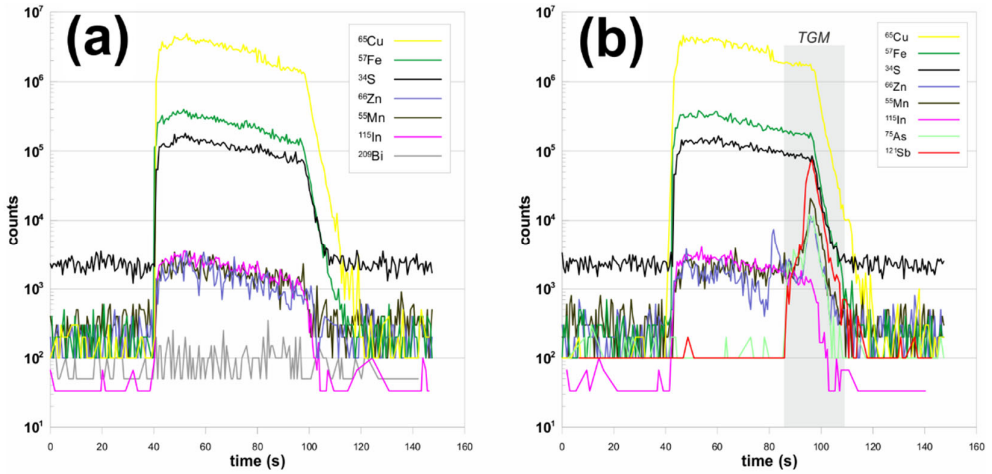

Figure 11. Selected time-resolved laser ablation ICP-MS depth profiles of chalcopyrite and associated inclusions (highlighted in grey) from the Kizhnica quarry: (**a**) flat spectra of chalcopyrite; (**b**) flat spectra of chalcopyrite; spiky patterns of Sb, As, and Zn could suggest the occurrence of tetrahedrite group minerals (TGM) inclusion.

4.1.4. Sphalerite

Sphalerite is relatively rare and is mainly observed in a pyrite-galena-quartz brecciated vein (Figure 4i) and in some polymetallic veinlets in the quarry. Sphalerite forms subhedral crystals up to 500 μm in association with galena and chalcopyrite. Some sphalerite crystals are crosscut by younger TGM veinlets, as well as secondary covellite. Additionally, minor tiny chalcopyrite exsolutions are also observed in some zones in sphalerite. The sphalerite formula can be expressed as $(Zn_{0.85–0.97}Fe_{0.01–0.14}Cu_{0.00–0.01}In_{0.00–0.01})_{\Sigma 1}S_{1.00–1.03}$. Two sphalerite crystals from the breccia mass were selected for measurement using LA-ICP-MS (Table 4). The first is characterized by high content of Fe (up to 43,200 ppm) and Cd (up to 2530 ppm), while the second grain is characterized by lower content of Fe (up to 9724 ppm) and a much higher content of Cu (up to 3717 ppm), In (up to 1655 ppm), and Sn (up to 1895 ppm). Significant positive correlations ($R > 0.94$) are observed between Cu, In, Sn, and Hg, while Fe and Mn have a strong negative correlation ($R < -0.78$) with the four elements mentioned earlier. Flat LA-ICP-MS spectra (Figure 12c,d) and the positive correlations between elements such as Cd, Cu, In, Sn, Hg, or Sb suggest that they are incorporated into the structure of sphalerite.

Table 4. LA-ICP-MS analyses of chalcopyrite, sphalerite, and tetrahedrite from Kizhnica quarry and arsenopyrite from hornfels. Values are in ppm, Fe in wt. % for chalcopyrite and arsenopyrite (microprobe), Zn in wt. % for sphalerite (microprobe), and Cu in wt. % for tetrahedrite (microprobe).

Mineralization Type	Hydrothermal Veinlets											Hornfels				
	Veinlets (n = 14); Chalcopyrite (Ccp)					Disseminated (n = 6); Sphalerite (Sph)					Veinlets (n=1); Tetrahedrite	Disseminated (n =10); Arsenopyrite 1 (Apy1)				
Element	**MIN**	**MAX**	**ST DEV**	**AVG**	**$n_{a.d.l.}$**	**MIN**	**MAX**	**ST DEV**	**AVG**	**$n_{a.d.l.}$**		**MIN**	**MAX**	**ST DEV**	**AVG**	**$n_{a.d.l.}$**
Ti	9.55	24	4.93	14	11	8.50	9.78	0.57	8.96	4	b.d.l.	42	3509	1201	1037	8
V	b.d.l.	b.d.l.	n.c.	n.c.	0	b.d.l.	b.d.l.	n.c.	n.c.	0	b.d.l.	2.90	24	9.06	13	9
Cr	23	37	4.97	28	10	5.53	5.53	n.c.	n.c.	1	b.d.l.	48	120	39	76	3
Mn	26	31	1.33	28	14	18	329	125	174	6	5.60	25	60	10	37	10
Fe	30.14	30.61	0.12	30.46	14	4309	43,188	18,299	30,493	6	10,421	29.43	33.75	1.23	31.93	10
Co	0.48	0.58	0.07	0.53	2	b.d.l.	b.d.l.	n.c.	n.c.	0	18	11,159	20,282	2960	16,011	10
Ni	b.d.l.	b.d.l.	n.c.	n.c.	0	b.d.l.	b.d.l.	n.c.	n.c.	0	b.d.l.	3205	15,365	4476	6865	10
Cu	372,279	426,230	14,482	405,036	14	185	3717	1413	1565	6	40.15	25	25	n.c.	n.c.	1
Zn	117	359	79	242	14	57.75	64.69	2.94	61.00	6	97,254	b.d.l.	b.d.l.	n.c.	n.c.	0
Ga	b.d.l.	b.d.l.	n.c.	n.c.	0	3.62	12	3.23	8.34	6	2.40	11	11	n.c.	n.c.	1
Ge	b.d.l.	b.d.l.	n.c.	n.c.	0	2.50	7.27	2.32	4.70	5	8.83	31	51	7.16	41	10

As	b.d.l.	b.d.l.	n.c.	n.c.	0	1.38	10	4.13	4.46	4	84,912	327,229	574,790	66,586	433,605	10
Se	b.d.l.	b.d.l.	n.c.	n.c.	0	b.d.l.	b.d.l.	n.c.	n.c.	0	b.d.l.	41	41	n.c.	n.c.	1
Mo	1.85	1.85	n.c.	n.c.	1	b.d.l.	b.d.l.	n.c.	n.c.	0	b.d.l.	7.93	7.93	n.c.	n.c.	1
Ag	b.d.l.	b.d.l.	n.c.	n.c.	0	0.65	2.36	0.65	1.13	6	150	b.d.l.	b.d.l.	n.c.	n.c.	0
Cd	4.21	4.21	n.c.	n.c.	1	1364	2530	428	1857	6	300	b.d.l.	b.d.l.	n.c.	n.c.	0
In	10	25	4.09	17	14	2.55	1655	832	556	6	7.65	0.37	0.72	0.12	0.53	10
Sn	b.d.l.	b.d.l.	n.c.	n.c.	0	21	1895	714	611	6	b.d.l.	2.98	2.98	n.c.	n.c.	1
Sb	b.d.l.	b.d.l.	n.c.	n.c.	0	13	94	28	41	6	174,331	8.05	22	4.60	13	10
Te	b.d.l.	b.d.l.	n.c.	n.c.	0	b.d.l.	b.d.l.	n.c.	n.c.	0	b.d.l.	28	28	n.c.	n.c.	1
W	b.d.l.	b.d.l.	n.c.	n.c.	0	0.79	0.79	n.c.	n.c.	1	b.d.l.	3.65	6.69	2.15	5.17	2
Au	0.28	0.28	n.c.	n.c.	1	b.d.l.	b.d.l.	n.c.	n.c.	0	b.d.l.	b.d.l.	b.d.l.	n.c.	n.c.	0
Hg	0.73	0.96	0.13	0.81	2	19	40	8.31	25	6	30	b.d.l.	b.d.l.	n.c.	n.c.	0
Pb	0.53	1.81	0.51	1.17	9	4.29	19	5.72	7.67	6	2609	1.27	4.68	1.25	2.84	7
Bi	0.35	7.09	2.19	1.26	9	0.16	0.16	n.c.	n.c.	1	31	13	313	91	61	10

Ta and Tl are below minimum detection limit. AVG = average value; b.d.l. = below detection limit; MIN = minimum value; MAX = maximum value; n = number of analyses; $n_{a.d.l.}$ = number of analyses above detection limit; n.c. = not calculated; STDEV = standard deviation.

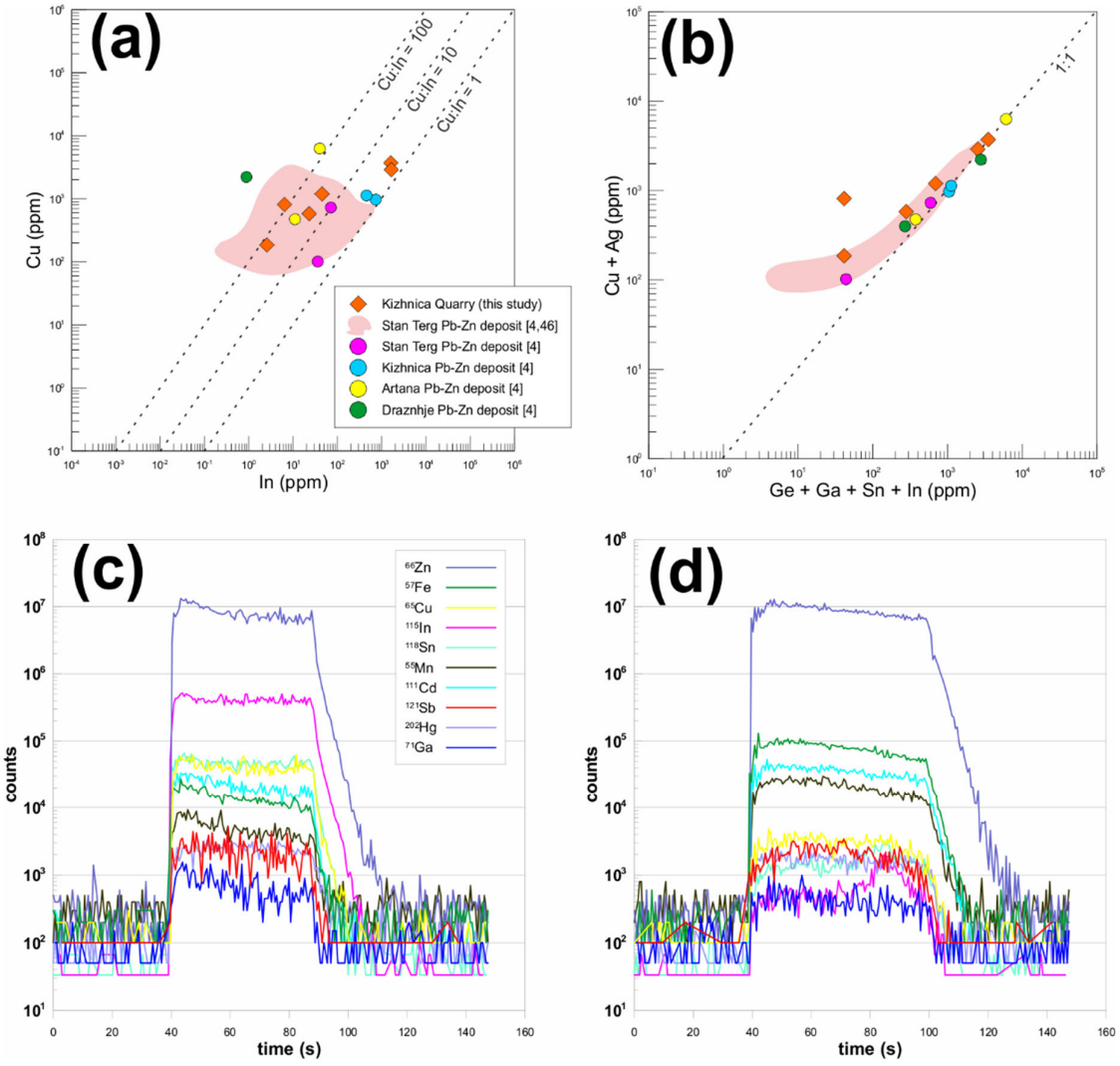

Figure 12. Binary plots showing the chemical composition of sphalerite from the Kizhnica quarry and selected Pb-Zn deposits from Kosovo (**a**,**b**) [4,46]**;** selected time-resolved laser ablation ICP-MS depth profiles of sphalerite from the Kizhnica quarry (**c**-**d**): (**a**) Cu vs In (in ppm); (**b**) Cu+Ag vs Ge+Ga+Sn+In (in ppm); (**c**) flat spectra of In,Sn,Cu-rich sphalerite; (**d**) flat spectra of sphalerite.

Tin enrichment in sphalerite from several Pb-Zn deposits within the Trepça Mineral Belt area, with concentrations up to several thousand ppm, was described by Kołodziejczyk et al. [4]. The content of Sn in sphalerite from the Kizhnica Pb-Zn deposit is 663 ppm, and in other deposits, Sn reaches up to 2800 ppm (Drazhnje), 1600 ppm (Artana), and up to 520 ppm (Stan Terg). On the other hand, the In content is not as high as the co-occurring Sn, reaching a maximum of 40 ppm in the Artana sphalerite. Only sphalerite from the Kizhnica Pb-Zn deposit reveals significant In content: up to 730 ppm [4]. In addition, high In contents in sphalerite (up to 0.75 wt.%) were described within listvenites from Kizhnica-Badovc [35]. Thus far, the mechanisms of In incorporation in sphalerite proposed in the literature depend on coupled substitutions: $2Zn^{2+} \leftrightarrow Cu^{+} + In^{3+}$ [47–50]; $3Zn^{2+} \leftrightarrow In^{3+} + Sn^{3+} + \square$ [51]; $3Zn^{2+} \leftrightarrow In^{3+} + (Cu,Ag)^{+} + Sn^{2+}$ [52]; and $4Zn^{2+} \leftrightarrow In^{3+} + Sn^{4+} + (Cu,Ag)^{+} + \square$ [52]. High In values in one sphalerite grain show a strong correlation with Cu (Figure 12a), and the data in the Cu vs In plot aligns 1:1 (Figure 12a). However, In also correlates well with Sn, and Sn with Cu, which would indicate the more complex substitution proposed by Frenzel et al. [52]: $In^{3+} + (Cu,Ag)^{+} + Sn^{2+} \leftrightarrow 3Zn^{2+}$. In addition, sphalerite from the Kizhnica quarry and other Pb-Zn deposits at Kosovo, as well as sphalerite from Dulong Zn–Sn–In skarn deposit from China [53], do not show a significant correlation between In and Ag. Consequently, Ag is of marginal importance in substitution at the position of a monovalent element. The correlation of monovalent Cu + Ag vs Sn + In + Ga + Ge aligns to the 1:1 ratio (Figure 12b) similarly to sphalerite from other Pb-Zn deposits from the Trepça Mineral Belt [4].

Contrary to most of the sphalerites from polymetallic deposits in Kosovo reported in the literature, the one from the quarry is characterized by significantly lower Fe content. Iron-rich sphalerite ("marmatite") from the Pb-Zn Stan Terg deposit has 9-15% wt.% of Fe [4,35,46]. High Fe contents were also determined at Artana Pb-Zn deposit (~11 wt.%) [4], the Pb-Zn Kizhnica deposit (~12 wt.%) [4], and the massive-banded and listvenite-type Zn-Pb-Sb ore from Kizhnica-Badovc (up to 22 wt.%) [35]. Similar to the Kizhnica quarry, lower contents were recorded at the Drazhnje Pb-Zn deposit (~2.6 wt.%). Relatively, low Fe contents would indicate lower crystallization temperatures than in the Badovc or Kizhnica deposits, located further to the west (Figure 2). The low-Fe content in sphalerite from the quarry and the mineral paragenesis in which it occurs suggests that it belongs to the Bi-Cu-Au mineralization (Figure 2) rather than to Pb-Zn-Ag mineralization.

LA-ICP-MS trace element data presented here were used to determine crystallization temperature of studied sphalerite by applying GGIMFis geothermometry (Ga, Ge, In, Mn, and Fe in sphalerite) [52], and the obtained results are in the range 253–269 °C. GGIMFis geothermometer applied to sphalerites from Badovc (quartz-sphalerite breccia and listvenites) shows significantly higher crystallization temperatures (330–390 °C) [20].

4.1.5. Tetrahedrite Group Minerals

Tetrahedrite group minerals (TGM) are observed as anhedral aggregates up to 200 μm in size within Cu-Bi veinlets in association with chalcopyrite and Bi-sulfosalts (Figure 4b). Additionally, TGM occurs as irregular clasts up to 500 μm within the pyrite-galena-quartz brecciated vein (Figure 4h). According to a new nomenclature and classification of tetrahedrite group minerals [54], both types of TGM from the Kizhnica quarry are the zinc members of the tetrahedrite and tennantite series (Figure 13b,c). Representative EPMA analyses of TGM are shown in Table 5.

Additionally, characteristic feature of TGM (tetrahedrite-(Zn) and tennantite-(Zn)) from the Kizhnica quarry is their Ag-poor character. A generalized formula for TGM from Cu-Bi veinlets based on 16 cations is $(Cu_{9.85\text{-}9.96}Ag_{0.00\text{-}0.01}Zn_{1.63\text{-}1.75}Fe_{0.29\text{-}0.56}Hg_{0.02\text{-}0.22})_{\Sigma=11.92–12.05}(Sb_{1.56–2.20}As_{1.84–2.48}Bi_{0.00–0.01})_{\Sigma=3.95–4.08}S_{12.85–13.10}$, with observed limited substitution at position *C* (e.g., Zn, Fe, Hg) and *D*-type constituents (Sb ↔ As) (Figure 13a,c).

A generalized formula for tetrahedrite-(Zn) from pyrite-galena-quartz vein based on 16 cations is $(Cu_{9.86–10.13}Zn_{1.24–1.83}Fe_{0.07–0.57}Hg_{0.02–0.22})_{\Sigma=12.04–12.17}(Sb_{3.17–3.71}As_{0.21–0.72}Bi_{0.01})_{\Sigma=3.83–}$

$_{3.96}S_{13.06–13.65}$. Small degree of Sb ↔ As substitution is observed in TGM from a pyrite-galena-quartz vein (Figure 13a,c). This TGM generation is characterized by *C* constituent variability at position C, where Zn dominates, but Fe and Hg incorporation is noteworthy (Figure 13b).

Only one TGM aggregate from Cu-Bi veinlets was sufficiently large to be measured with LA-ICP-MS (Table 4; Figure 13d). The analyzed TGM contains Pb (2609 ppm), Cd (300 ppm), Ag (150 ppm), Bi (31 ppm), Hg (30 ppm), Co (18 ppm), Ge (8.8 ppm), In (7.7 ppm), Mn (5.6 ppm), and Ga (2.4 ppm). Bi and In contents are relatively low compared to another Cu-Bi occurrence within the same Kizhnica ore field (Janjevo locality) [37]. Another distinctive feature is complete Sb ↔ As substitution within the macroscopic aggregates of TGM from Janjevo. In contrast to TGM from Janjevo, but in agreement with data from other known TGMs studied by George et al. [55], In from the Kizhnica quarry preferentially partitions into the co-crystallized sphalerite and chalcopyrite.

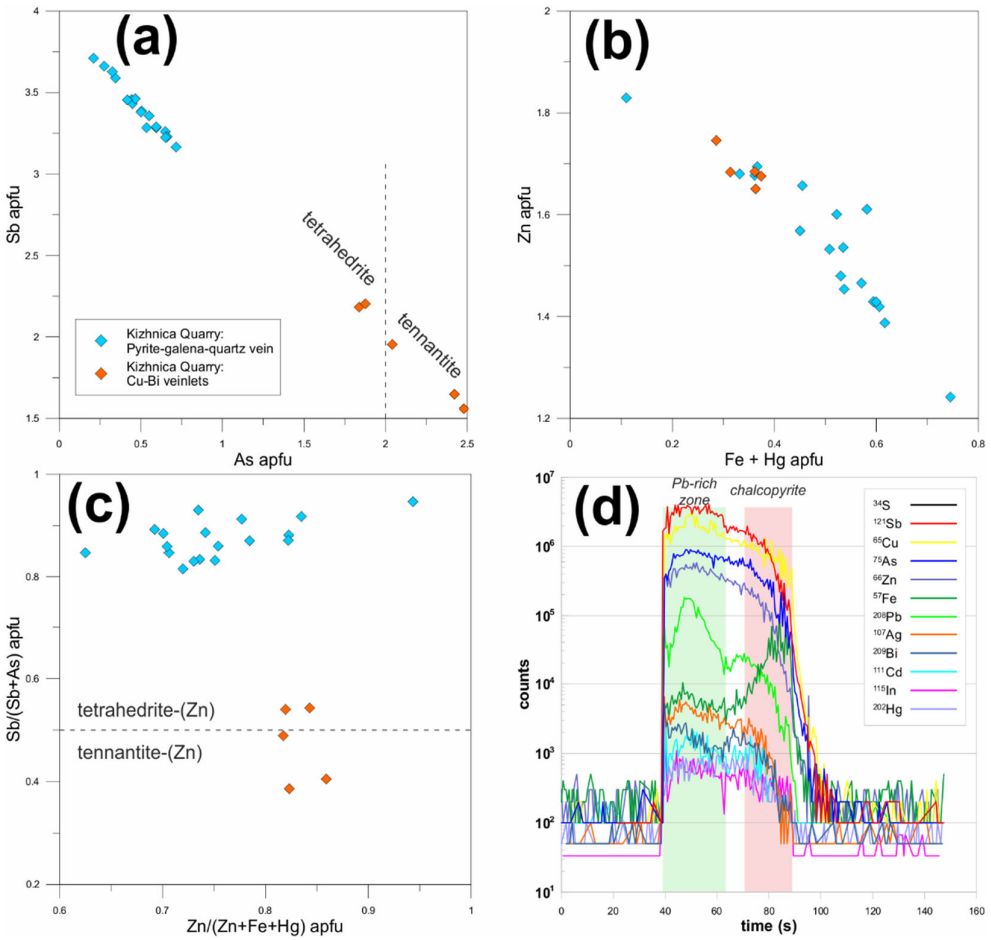

Figure 13. Compositional relationships in the tetrahedrite group minerals (TGM) from the Kizhnica quarry: (**a**) Sb vs As binary plot (apfu); (**b**) Zn vs Fe+Hg binary plot (apfu); (**c**) Sb/(Sb + As) vs Zn/(Zn + Fe + Hg) (apfu); (**d**) spectra of TGM with Pb-rich zone; increase in Fe is associated with the presence of chalcopyrite inclusion.

Table 5. Representative EPMA data for TGM: tetrahedrite-(Zn) [1–7] and tennantite-(Zn) [8–10] from Kizhnica quarry: polymetallic veinlets [1–6] and breccia [7–10], b.d.l. = below detection limit.

Analyses	wt.%										apfu Σ16 Cation								
	S	Cu	Sb	Bi	Fe	Zn	Hg	Ag	As	Total	S	Cu	Sb	Bi	Fe	Zn	Hg	Ag	As
1	25.58	38.55	26.73	0.10	1.03	6.65	0.32	0.02	1.48	100.44	13.18	10.02	3.63	0.01	0.31	1.68	0.03	0.00	0.33
2	25.85	39.12	25.52	0.11	1.92	5.67	0.52	0.04	2.05	100.78	13.20	10.08	3.43	0.01	0.56	1.42	0.04	0.01	0.45
3	25.80	38.94	25.10	0.10	1.18	6.76	0.26	0.04	2.29	100.45	13.19	10.04	3.38	0.01	0.34	1.69	0.02	0.01	0.50
4	25.72	38.86	24.28	0.08	1.80	5.67	0.78	b.d.l.	2.70	99.89	13.23	10.08	3.29	0.01	0.53	1.43	0.06	-	0.59
5	26.35	38.74	24.08	0.11	1.77	4.89	2.64	0.02	2.68	101.29	13.65	10.12	3.28	0.01	0.53	1.24	0.22	0.00	0.59
6	25.79	38.75	23.33	0.08	1.70	5.80	0.84	b.d.l.	3.25	99.55	13.29	10.07	3.17	0.01	0.50	1.47	0.07	-	0.72
7	26.64	40.15	16.86	0.13	1.11	6.99	b.d.l.	0.09	8.74	100.70	13.10	9.96	2.18	0.01	0.31	1.68	-	0.01	1.84
8	26.75	40.31	15.17	0.12	1.32	6.99	0.06	b.d.l.	9.75	100.46	13.09	9.95	1.95	0.01	0.37	1.68	0.00	-	2.04
9	26.75	40.44	12.92	0.14	1.03	7.35	b.d.l.	b.d.l.	11.68	100.32	12.96	9.89	1.65	0.01	0.29	1.75	-	-	2.42
10	26.85	41.01	12.37	0.08	1.32	7.18	b.d.l.	0.03	12.10	100.94	12.85	9.90	1.56	0.01	0.36	1.68	-	0.00	2.48

4.1.6. Associated minerals

Galena is widespread and occurs as euhedral or subhedral crystals up to a few cm in size (Figures 3a; 4i). Together with pyrite is the main component of pyrite-galena-quartz brecciated vein. Numerous galena inclusions are also observed in pyrite from Cu-Bi veinlets.

Hematite forms coarse crystalline aggregates (specularite) up to a few cm occurring in epithermal veinlets (Figure 3b,c). It occurs as numerous elongated euhedral crystals in veinlets with calcite (Figure 4a,c).

Marcasite is observed in the form of irregular clasts up to 200 μm in the pyrite-galena-quartz vein (Figure 4h).

Covellite is a secondary mineral found in the pyrite-galena-quartz vein. It replaced galena crystals and forms aggregates of up to 200 μm (Figure 4h,i).

4.2. Kizhnica Hornfels

The Bi-Au-Cu-Te mineralization forms disseminations in hornfels, which were formed at the contact of a flysch series and andesite dykes, north of the Kizhnica andesite quarry. Hornfels consists of Mg-Fe amphiboles, K-feldspar, and chlorites with minor quartz, apatite, titanite, and zircon. Mineralization occurs at the contact of silicates with irregular calcite lenses up to a few cm in size (Figure 3d–f; Figure 14a). The Bi-Au-Cu-Te mineralization is represented there by Bi sulfosalts (cannizzarite, bismuthinite, galenobismutite, and cosalite), sulfarsenides (arsenopyrite, gersdorffite, and cobaltite), sulfides (chalcopyrite, pyrite, sphalerite, pyrrhotite, and galena), native elements (native gold and bismuth), and tetradymite (Figures 14a–i and 15). Mineralization can be divided into three stages: (1) sulfarsenides, (2) sulfide, and (3) Bi-Au (Figure 15). The first stage is characterized by the evolution of sulfarsenides from Fe-member (Apy1), through Ni-Co members (gersdorffite-cobaltite), arsenopyrite 2 (Apy2) and pyrite. Base metal sulfides crystallized subsequently. The Bi-Au period was initiated by the crystallization of native gold, native bismuth, tetradymite, and bismuthinite. Then Bi-Pb sulfosalts such as cannizzarite, cosalite, and galenobismutite formed (Figure 15).

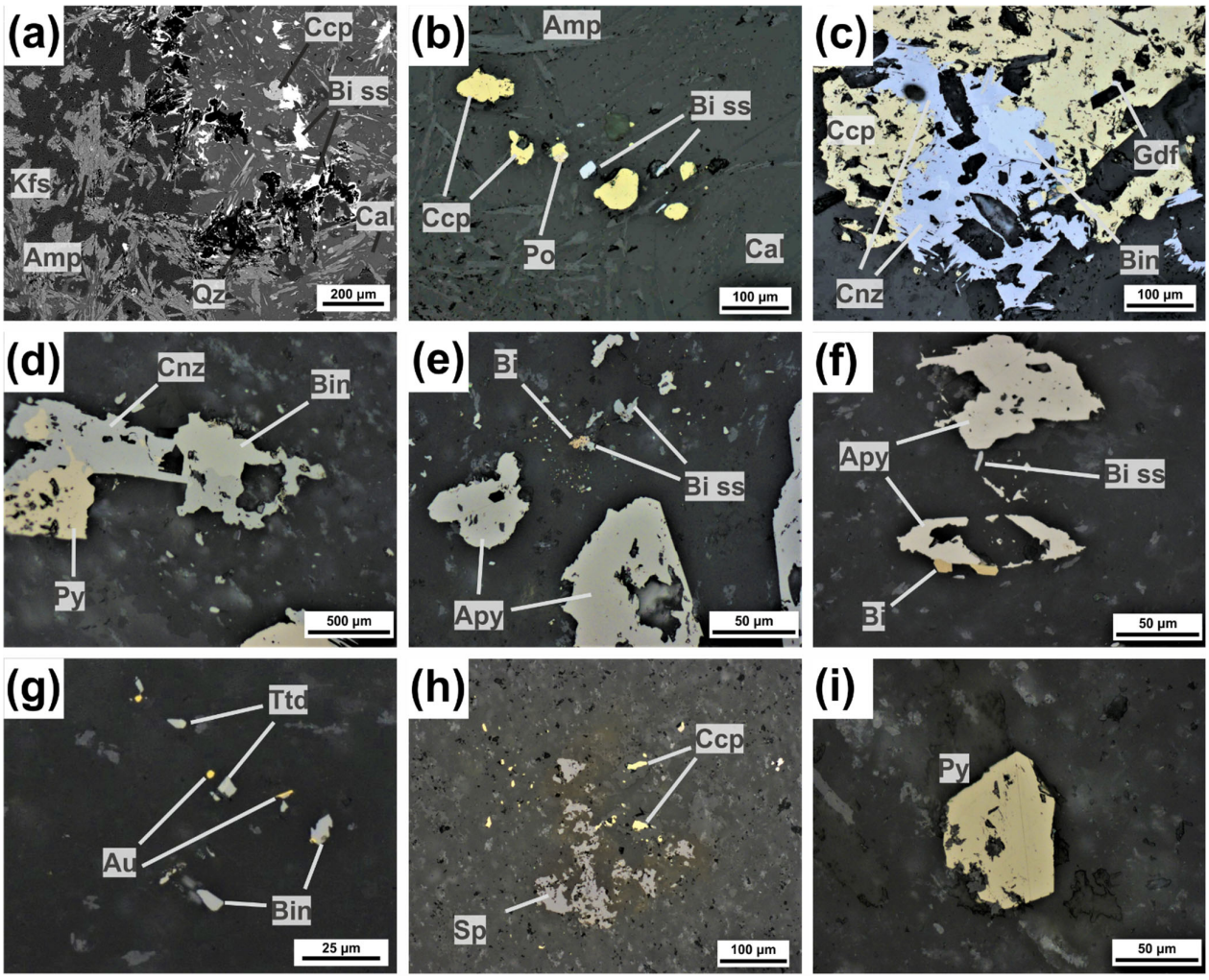

Figure 14. Back-scattered electron (BSE) image (**a**) and reflected-light photomicrographs (**b–i**) of Bi-Au-Cu-Te mineralization from the Kizhnica hornfels: (**a**) irregular aggregates of chalcopyrite and Bi sulfosalts at the contact of calcite with K-feldspar, quartz, and amphibole; (**b**) chalcopyrite associated with pyrrhotite and Bi sulfosalts disseminated in hornfels matrix composed of calcite and amphibole; (**c**) chalcopyrite with cannizzarite–bismuthinite aggregate and gersdorffite inclusion; (**d**) aggregate of cannizzarite with bismuthinite replacing pyrite; (**e**) disseminated native bismuth droplets and bismuth sulfosalts in hornfels matrix near arsenopyrite crystals; (**f**) native bismuth and Bi sulfosalts overgrowing arsenopyrite; (**g**) disseminated tiny crystals of native gold, tetradymite, and bismuthinite; (**h**) sphalerite–chalcopyrite aggregate; (**i**) euhedral pyrite crystal. Abbreviations: Amp = amphibole; Apy = arsenopyrite; Au = native gold; Bi = native bismuth; Bi ss = bismuth sulfosalts; Bin = bismuthinite; Cal = calcite; Ccp = chalcopyrite; Cnz = cannizzarite; Gdf = gersdorffite; Kfs = K-feldspar; Qz = quartz; Po = pyrrhotite; Py = pyrite; Sp = sphalerite; Ttd = tetradymite.

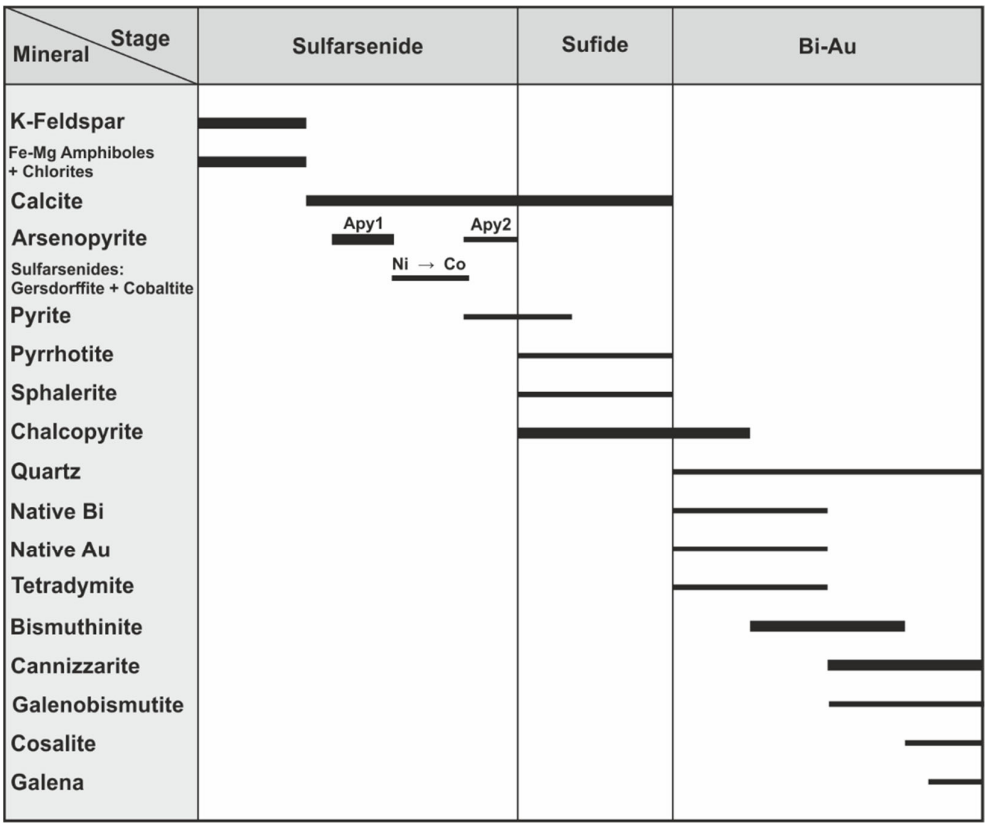

Figure 15. Formation stages and paragenetic sequence of Bi-Au-Cu-Te mineralization from the Kizhnica hornfels.

4.2.1. Bismuth Sulfosalts

Bismuthinite-aikinite series

Bismuthinite is a common Bi sulfosalt in Kizhnica hornfels. It is most often found as disseminated euhedral or subhedral crystals up to 300 μm (Figures 14b; 16a) or aggregates with cannizzarite (Figures 14c–e; 16b–d), less often with galenobismutite (Figure 16e). In some cases, it overgrows pyrite and arsenopyrite crystals (Figure 14f). Surrounded by a light-gray cannizzarite, bismuthinite is a medium grey with a characteristic greenish tint in reflected light (Figure 14c–d). Cannizzarite and galenobismutite usually overgrow bismuthinite. The degree of aikinite type substitution (n_{aik}) in bismuthinite from hornfels is 1.76–5.73 (Figure 6), which is significantly lower than in the quarry samples. The formula of bismuthinite can be expressed as $(Bi_{7.60–7.90}Pb_{0.07–0.24}Cu_{0.06–0.23}Fe_{0.00–0.20}Sb_{0.01–0.06})_{\Sigma 7.74-8.67}S_{11.21-12.57}$ (Table 6). Bismuthinite in hornfels has slightly higher Sb (up to 0.34 wt.%) and Ag (up to 0.06 wt.%) content in comparison to bismuthinite from the Kizhnica quarry.

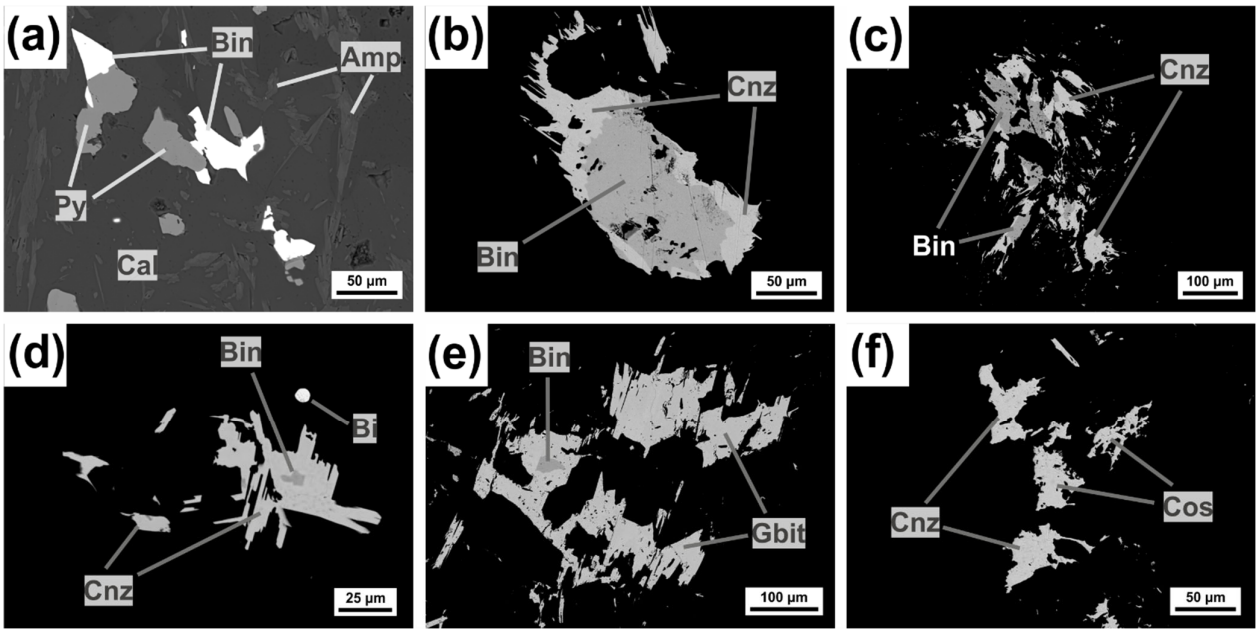

Figure 16. Back-scattered electron (BSE) images showing Bi sulfosalts from the Kizhnica hornfels: (**a**) bismuthinite overgrowing pyrite aggregates in hornfels matrix composed of calcite and amphibole; (**b**) cannizzarite overgrowing bismuthinite; (**c**) aggregate of cannizzarite with bismuthinite; (**d**) euhedral cannizzarite crystal with bismuthinite in the center and disseminated native bismuth droplet; (**e**) galenobismutite euhedral crystals with bismuthinite; (**f**) cosalite and cannizzarite crystals. Abbreviations: Amp = amphiboles; Bi = native bismuth; Bin = bismuthinite; Cal = calcite; Cnz = cannizzarite; Cos = cosalite; Gbit = galenobismutite; Py = pyrite.

Table 6. Representative EPMA data for bismuthinite from the Kizhnica hornfels. The empirical formula was calculated based on the sum Ag + Bi + Sb + Fe + As + (Pb + Cu)/2 = 8 atoms, b.d.l. = below detection limit.

Analyses	wt.%									apfu								Cations	n_{aik}
	S	Fe	Cu	Ag	Sb	Pb	As	Bi	Total	S	Fe	Cu	Ag	Sb	Pb	As	Bi		
1	**19.20**	b.d.l.	0.36	b.d.l.	0.24	0.66	b.d.l.	79.24	99.77	12.41	-	0.12	-	0.04	0.07	-	7.86	8.09	2.21
2	19.26	b.d.l.	0.37	b.d.l.	0.26	0.66	b.d.l.	79.23	99.86	12.43	-	0.12	-	0.04	0.07	-	7.84	8.09	2.42
3	19.05	b.d.l.	0.35	b.d.l.	0.22	1.56	b.d.l.	78.76	99.96	12.33	-	0.11	-	0.04	0.16	-	7.82	8.13	3.33
4	19.03	b.d.l.	0.57	b.d.l.	0.22	1.48	b.d.l.	77.78	99.09	12.42	-	0.19	-	0.04	0.15	-	7.79	8.17	4.08
5	18.89	b.d.l.	0.58	b.d.l.	0.18	1.30	b.d.l.	78.52	99.54	12.23	-	0.19	-	0.03	0.13	-	7.80	8.16	4.21
6	19.12	b.d.l.	0.58	b.d.l.	0.20	2.00	b.d.l.	77.90	99.81	12.43	-	0.19	-	0.03	0.20	-	7.77	8.20	4.74
7	18.93	b.d.l.	0.68	b.d.l.	0.22	1.57	0.20	77.75	99.37	12.24	-	0.22	-	0.04	0.16	0.03	7.71	8.17	4.80
8	18.89	b.d.l.	0.70	b.d.l.	0.21	2.37	0.23	77.43	99.84	12.19	-	0.23	-	0.04	0.24	0.04	7.67	8.21	5.73

Cannizzarite

Cannizzarite is the most common Bi sulfosalt in the studied material and occurs as euhedral needle-like crystals up to 400 µm, frequently in association with bismuthinite (Figures 14c–e; 16b–d). The analyzed samples typically contain only Pb, Bi, and S; small admixtures of other minor elements such as Fe, Cu, Ag, As, and Sb are rare. The formula of cannizzarite from Kizhnica hornfels based on 104 cations [56] can be expressed as $(Pb_{46.62–48.92}Fe_{0.00–0.82}Cu_{0.00–0.42}Ag_{0.00–0.40})_{\Sigma 47.15-49.53}(Bi_{54.41–56.62}As_{0.00–0.56}Sb_{0.01–0.33})_{\Sigma 54.14-56.85}S_{130.58-136.68}$ (Table 7; Figure 7). The chemical composition of cannizzarite (member of variable-fit homologous series) found in nature is highly variable and could strongly diverge from the theoretical formula $Pb_{48}Bi_{56}(S_{124}Se_8)_{132}$ proposed by Topa et al. [56] for samples from the type locality Vulcano (the Aeolian Islands, Southern Italy). Additionally, end members of the cannizzarite series have been reported from two localities: (1) 7H:12Q homologue from the Vulcano [56] and (2) 3H:5Q from the Kudriavy Volcano, on Iturup Island, Kurile Archipelago, Russia [57]. Previous studies [58–61] carried out on cannizzarite and

coexisting Se-rich variant wittite $Pb_9Bi_{12}(S,Se)_{27}$ from fumaroles at Vulcano provided data on, e.g., $S^{2-} \leftrightarrow Se^{2-}$ substitution. The presence of Se in cannizzarite was also described from Au-Cu-Bi assemblage from the Obari Mine, Yamagata Prefecture Japan [62]. On the other hand, several hydrothermal occurrences with Se-free cannizzarite have been reported, e.g., Felbertal, Austria [63]; Kram locality, Boranja ore field, Serbia [11]; and Stan Terg, Kosovo [15]. In addition, within cannizzarite, data presented here clearly show heterovalent Pb–Bi substitution, which affects the non-stoichiometric formulas of members of the series (Figure 17a). Cannizzarite from Kizhnica is characterized by similar Bi and Pb content in comparison with cannizzarite from the type locality, while cannnizzarite from other locations varies significantly (Figure 17a). Cannizzarite from Kizhnica shows variation in S content dependent on Pb-Bi substitution; the increase of Bi corresponds to S content increase (Figure 17c), whereas the increase of Pb corresponds to S content decrease (Figure 17b,d). Combined chemical data for all available cannizzarite in the literature reveal a similar trend (Figure 17b–d). The chemistry of the studied cannizzarite from Kizhnica hornfels is closest to that from Vulcano, which would suggest a genetic relationship directly related to the volcanic activity in Kizhnica. Cannizzarite from the studied hornfels occurs in an association similar to Vulcano's cannizzarite, where bismuthinite and galenobismutite occur in fumarole vents [60,61] and crystallized temperatures from 400 to 600 °C [60,64]. Based on sulphosalts association, cannizzarite in hornfels was crystallized in temperatures below 400 °C.

Table 7. Representative EPMA data for cannizzarite from the Kizhnica hornfels. The empirical formula was calculated based on the 104 cations [56], b.d.l. = below detection limit.

Analyses	wt.%									apfu								Anions
	S	Fe	Cu	Ag	Sb	Pb	As	Bi	Total	S	Fe	Cu	Ag	Sb	Pb	As	Bi	
1	16.72	0.11	0.06	b.d.l.	0.06	38.42	b.d.l.	44.61	100.26	134.53	0.52	0.23	-	0.14	47.85	-	55.08	134.53
2	16.69	0.10	b.d.l.	0.11	b.d.l.	37.92	b.d.l.	45.03	99.99	134.40	0.44	-	0.26	-	47.25	-	55.63	134.40
3	16.93	0.07	0.10	0.10	0.16	37.94	b.d.l.	44.48	99.94	136.65	0.32	0.41	0.23	0.33	47.39	-	55.09	136.65
4	16.57	b.d.l.	0.07	b.d.l.	0.06	38.40	b.d.l.	44.53	99.73	134.08	-	0.30	-	0.13	48.07	-	55.29	134.08
5	16.63	b.d.l.	0.10	0.10	0.06	38.03	b.d.l.	44.63	99.60	134.65	-	0.40	0.25	0.12	47.66	-	55.46	134.65
6	16.41	b.d.l.	0.07	0.12	0.07	38.41	b.d.l.	44.39	99.51	132.71	-	0.30	0.28	0.16	48.07	-	55.09	132.71
7	16.69	b.d.l.	0.08	b.d.l.	0.07	37.59	b.d.l.	44.74	99.32	135.97	-	0.33	-	0.16	47.37	-	55.91	135.97
8	16.65	b.d.l.	0.08	b.d.l.	0.13	38.02	b.d.l.	44.36	99.30	135.64	-	0.31	-	0.27	47.93	-	55.45	135.64
9	16.61	0.18	0.05	0.15	b.d.l.	37.36	b.d.l.	44.86	99.28	134.53	0.82	0.20	0.36	-	46.82	-	55.73	134.53
10	16.53	b.d.l.	0.06	b.d.l.	0.09	37.84	b.d.l.	44.47	99.11	134.65	-	0.25	-	0.20	47.69	-	55.57	134.65
11	16.38	b.d.l.	0.10	b.d.l.	0.07	38.00	b.d.l.	44.40	99.10	133.16	-	0.42	-	0.14	47.79	-	55.36	133.16
12	16.45	b.d.l.	0.09	0.10	0.06	38.62	b.d.l.	43.75	99.09	133.80	-	0.37	0.23	0.13	48.60	-	54.58	133.80

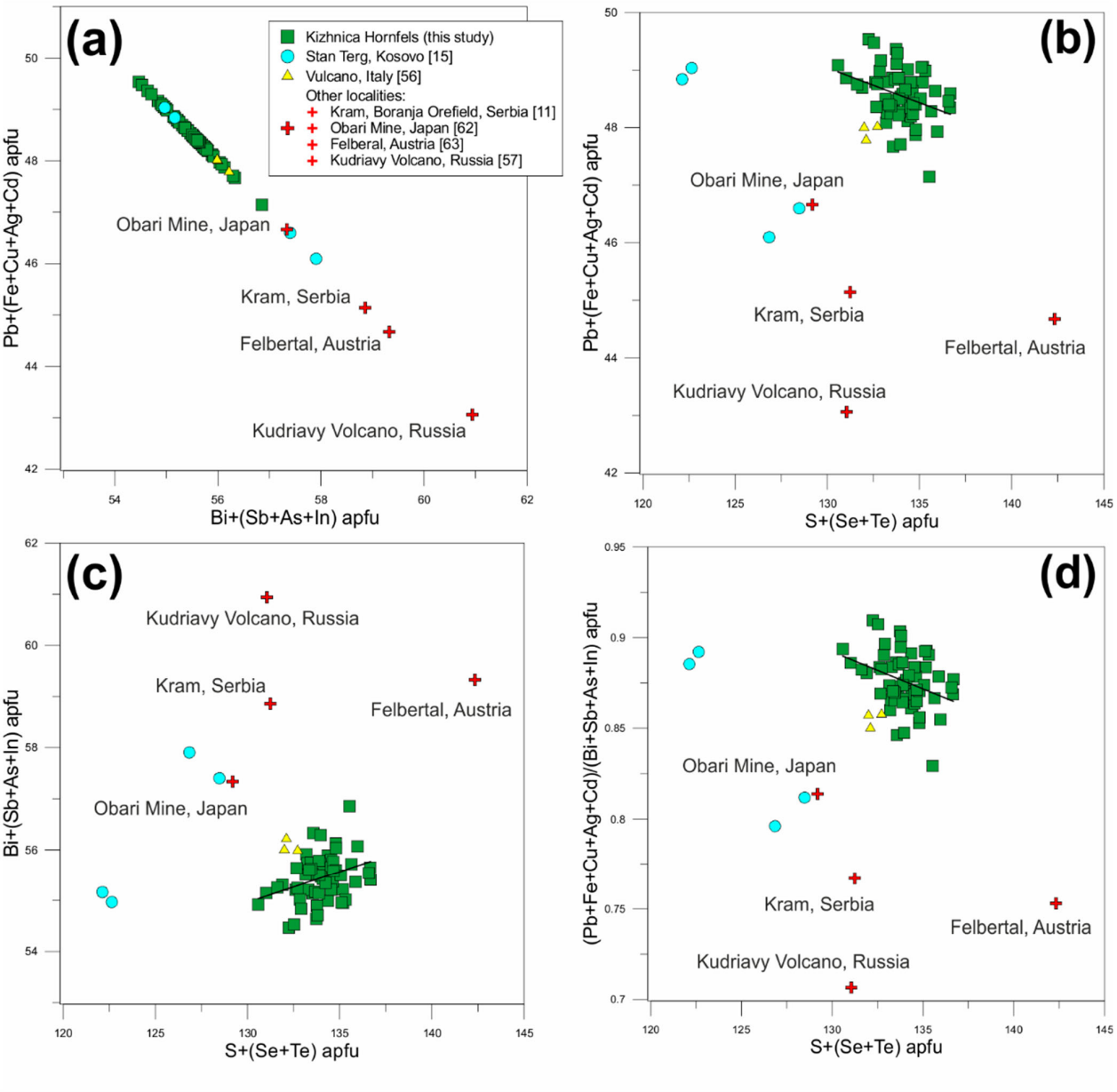

Figure 17. Binary plots showing the chemical composition of cannizzarite from the Kizhnica hornfels and known locations of cannizzarite from the literature [11,15,56,57,62,63]: (**a**) Pb + (Fe + Cu + Ag + Cd) vs Bi + (Sb + As + In) (apfu); (**b**) Pb + (Fe + Cu + Ag + Cd) vs S + (Se + Te) (apfu); (**c**) Bi + (Sb + As + In) vs S + (Se + Te) (apfu); (**d**); (Pb + Fe + Cu + Ag + Cd)/(Bi + Sb + As + In) vs S + (Se + Te) (apfu).

Galenobismutite

Galenobismutite occurs as euhedral or subhedral crystals up to 300 μm in size, associated with bismuthinite (Figure 16e). The chemical composition of galenobismutite and the corresponding chemical formulae are given in Table 8. The chemical composition of galenobismutite is close to the ideal formula; only traces of Sb (up to 0.17 wt.%) and As (up to 0.14 wt.%) were identified. The generalized formula based on 3 cations can be expressed as $(Pb_{0.97–1.05}Bi_{1.95–2.02})_{\Sigma 3.00}S_{\Sigma 3.81–4.13}$ (Table 8; Figure 7).

Table 8. Representative EPMA data for galenobismutite from the Kizhnica hornfels. The empirical formula was calculated based on 3 cations, b.d.l. = below detection limit.

Analyses	wt.%									apfu								Cations
	S	Fe	Cu	Ag	Sb	Pb	As	Bi	Total	S	Fe	Cu	Ag	Sb	Pb	As	Bi	
1	16.97	b.d.l.	b.d.l.	b.d.l.	0.10	28.54	b.d.l.	54.31	99.97	3.98	-	-	-	0.01	1.04	-	1.95	3.00
2	17.25	b.d.l.	b.d.l.	b.d.l.	0.05	27.74	0.14	54.54	99.76	4.06	-	-	-	0.00	1.01	0.01	1.97	3.00
3	17.27	b.d.l.	0.07	b.d.l.	0.09	27.63	b.d.l.	54.57	99.62	4.08	-	0.01	-	0.01	1.01	-	1.98	3.00
4	17.16	b.d.l.	b.d.l.	b.d.l.	-	28.23	b.d.l.	54.17	99.57	4.06	-	-	-	-	1.03	-	1.97	3.00
5	17.44	b.d.l.	b.d.l.	b.d.l.	0.10	28.03	b.d.l.	53.87	99.56	4.13	-	-	-	0.01	1.03	-	1.95	3.00
6	17.14	b.d.l.	b.d.l.	b.d.l.	0.15	28.01	b.d.l.	54.12	99.41	4.05	-	-	-	0.01	1.03	-	1.96	3.00
7	17.33	0.10	b.d.l.	b.d.l.	0.07	27.99	b.d.l.	53.90	99.40	4.10	0.01	-	-	0.00	1.02	-	1.96	3.00
8	17.32	b.d.l.	b.d.l.	b.d.l.	0.12	28.40	b.d.l.	53.51	99.36	4.11	-	-	-	0.01	1.04	-	1.95	3.00
9	17.37	b.d.l.	b.d.l.	b.d.l.	0.13	28.09	b.d.l.	53.71	99.33	4.12	-	-	-	0.01	1.03	-	1.96	3.00
10	17.28	b.d.l.	b.d.l.	b.d.l.	0.07	28.20	b.d.l.	53.71	99.31	4.10	-	-	-	0.00	1.04	-	1.96	3.00

Cosalite

Cosalite was found only in one sample as subhedral crystals 60 μm in width in association with cannizzarite (Figure 16f). In reflected light and BSE images, it is indistinguishable from cannizzarite. The chemical composition of cosalite is relatively uniform and close to the ideal formula with only traces of Cu (up to 0.41 wt.%) and Sb (up to 0.18 wt.%). The formula of cosalite based on 20 anions [41] can be expressed as $(Cu_{0.21–0.25})_{\Sigma 0.21–0.25}(Pb_{7.70–7.79}Fe_{0.04–0.06})_{\Sigma 7.76–7.84}(Bi_{7.50–7.65}Sb_{0.05–0.06})_{\Sigma 7.57–7.70}S_{\Sigma 20}$ (Table 9; Figure 7). Following the general formula for cosalite—$Cu_xAg_{i+s}Pb_{8–2s–0.5(x+i)}Bi_{8+s}S_{20}$ proposed by Topa and Makovicky [41], only 2Cu ↔ Pb substitution is present in the analyzed samples, with x content in the range from 0.21 up to 0.25. 2(Cu + Ag) ↔ Pb substitution described by Topa and Makovicky [41] as well as Ag + Bi ↔ 2Pb (lillianite type of substitution) being negligible described as Ag is absent here. Content of trivalent elements (Bi + Sb + As) in cosalite is close to the ideal 8 apfu (range 7.57 up to 7.7) showing a lack of other substitution for Bi in cosalite structure. Cosalite has a low range of Sb vs Bi substitution—the content of Sb is up to 0.15 wt.%. In comparison with epithermal cosalite from the Kizhnica quarry, hornfels cosalite is similar to the skarn cosalite known from the Serbo-Macedonian metallogenic province (Rudnik, Kram, and Stan Terg) [11,16,42] (Figure 8 a–c).

Table 9. Representative EPMA data for cosalite from the Kizhnica hornfels. The empirical formula was calculated based on 20 anions.

Analyses	wt.%									apfu								Cations
	S	Fe	Cu	Ag	Sb	Pb	As	Bi	Total	S	Fe	Cu	Ag	Sb	Pb	As	Bi	
1	16.61	0.07	0.40	b.d.l.	0.17	41.82	b.d.l.	41.39	100.46	20.00	0.05	0.24	-	0.05	7.79	-	7.65	15.78
2	16.64	0.06	0.41	b.d.l.	0.15	41.82	b.d.l.	40.68	99.87	20.00	0.04	0.25	-	0.05	7.78	-	7.50	15.66
3	16.45	0.09	0.34	b.d.l.	0.18	40.91	b.d.l.	40.94	98.94	20.00	0.06	0.21	-	0.06	7.70	-	7.64	15.68

4.2.2. Sulfarsenides: Arsenopyrite-Gersdorffite-Cobaltite

Sulfarsenides were often encountered in the studied samples. Three generations of sulfarsenides (Fe-Ni-Co) can be distinguished: (1) early arsenopyrite (Apy1), (2) gersdorffite-cobaltite, and (3) younger arsenopyrite (Apy2).

Early arsenopyrite (Apy1) is the most abundant ore mineral observed in the studied samples and forms euhedral or subhedral crystals up to 500 μm disseminated in hornfels rock (Figures 14c,f; 18a,b). Arsenopyrite (Apy1) crystals are often very corroded, overgrown by younger arsenopyrite (Apy2) and Bi sulfosalts, and contain inclusions of Mg-Fe amphiboles and calcite. The formula of arsenopyrite (Apy1) can be expressed as $(Fe_{0.76–0.98}Co_{0.01–0.16}Ni_{0.01–0.08})_{\Sigma 1}As_{1.01–1.11}S_{0.82–0.91}$ (Table 10). Early arsenopyrite displays a Co + Ni substitutional trend on the ternary Ni-Co-Fe diagram (Figure 19a), related to the sub-

stitution of Fe by Co and Ni (Co + Ni: up to 0.24 apfu). Apy1 is enriched in As (1.01–1.11 apfu) and depleted in S (0.82–0.91 apfu) in comparison with stoichiometric arsenopyrite (Figure 19b); the As/S ratio varies from 1.13 to 1.35 (Figure 19c). BSE images show irregular zonation caused by the As ↔ S substitution (Figure 18b). Additionally, the outer parts of arsenopyrite crystals are replaced by younger arsenopyrite (Apy2) with higher S content (Figure 18b).

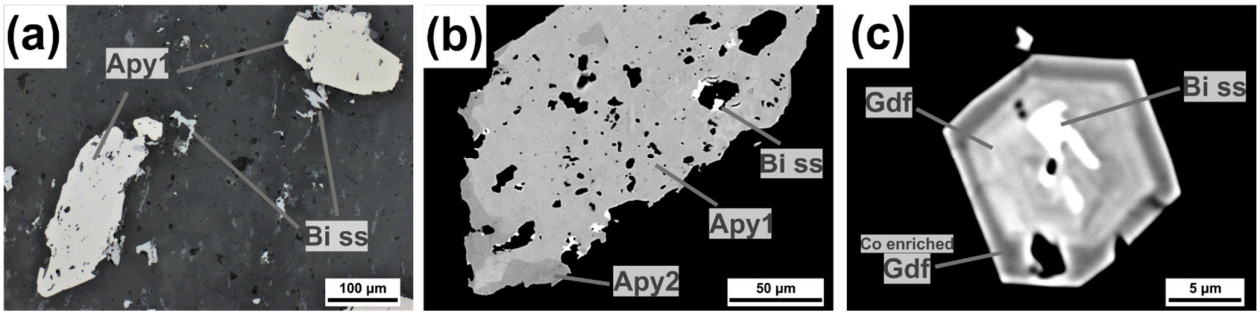

Figure 18. Reflected-light image (**a**) and back-scattered electron (BSE) images (**b**,**c**) showing sulfarsenides from the Kizhnica hornfels: (**a**) early arsenopyrite with younger Bi sulfosalts crystals; (**b**) corroded and porous early arsenopyrite crystal containing Bi sulfosalts inclusions with younger arsenopyrite crystallized in the outer zones; (**c**) inclusions of Bi sulfosalts in euhedral gersdorffite crystal with regular zonation and outer zone enriched in Co. Abbreviations: Apy = arsenopyrite; Bi ss = bismuth sulfosalts; Gdf = gersdorffite.

Table 10. Representative EPMA data for sulfarsenides: early arsenopyrite (Apy1) [1–9], cobaltite [10,11], gersdorffite [12–15], and younger arsenopyrite (Apy2) [16–20] from the Kizhnica hornfels, b.d.l. = below detection limit.

Analyses	wt.%								apfu Σ1 Cation							Cations	Anions	As/S
	Fe	Ni	Co	As	Sb	Bi	S	Total	Fe	Ni	Co	As	Sb	Bi	S			
1	**32.18**	**1.77**	0.35	48.32	0.05	0.02	17.23	99.94	0.94	0.05	0.01	1.05	0.00	0.00	0.88	1.00	1.93	1.20
2	30.81	1.50	1.60	49.72	b.d.l.	b.d.l.	15.88	99.55	0.91	0.04	0.04	1.10	-	-	0.82	1.00	1.92	1.34
3	32.54	0.53	1.61	47.02	b.d.l.	b.d.l.	17.52	99.29	0.94	0.01	0.04	1.01	-	-	0.88	1.00	1.90	1.15
4	32.71	0.29	1.83	47.88	b.d.l.	b.d.l.	17.29	100.05	0.94	0.01	0.05	1.03	-	-	0.87	1.00	1.90	1.19
5	30.66	1.03	2.10	49.47	b.d.l.	b.d.l.	15.94	99.20	0.91	0.03	0.06	1.10	-	-	0.83	1.00	1.92	1.33
6	30.81	0.66	2.24	49.86	b.d.l.	b.d.l.	15.75	99.36	0.92	0.02	0.06	1.11	-	-	0.82	1.00	1.93	1.35
7	30.90	0.88	2.89	47.30	b.d.l.	b.d.l.	17.94	99.91	0.90	0.02	0.08	1.02	-	-	0.91	1.00	1.93	1.13
8	29.66	1.34	3.43	47.68	b.d.l.	b.d.l.	17.11	99.22	0.87	0.04	0.10	1.04	-	-	0.87	1.00	1.91	1.19
9	26.10	2.75	5.79	48.63	b.d.l.	b.d.l.	16.73	100.03	0.76	0.08	0.16	1.06	-	-	0.85	1.00	1.91	1.24
10	9.10	13.04	13.88	44.00	b.d.l.	b.d.l.	19.72	99.80	0.26	0.36	0.38	0.95	-	-	0.99	1.00	1.94	0.95
11	8.80	11.22	14.87	44.86	b.d.l.	0.02	19.78	100.50	0.26	0.32	0.42	1.00	-	0.00	1.03	1.00	2.02	0.97
12	8.35	23.15	2.39	50.26	b.d.l.	b.d.l.	15.26	99.43	0.26	0.67	0.07	1.15	-	-	0.81	1.00	1.96	1.41
13	9.78	20.08	3.56	48.40	b.d.l.	b.d.l.	16.86	99.70	0.30	0.59	0.10	1.12	-	-	0.91	1.00	2.03	1.23
14	9.57	13.81	12.48	44.01	b.d.l.	b.d.l.	19.67	99.55	0.28	0.38	0.34	0.95	-	-	0.99	1.00	1.94	0.96
15	8.86	13.61	13.46	44.28	b.d.l.	b.d.l.	19.21	99.47	0.26	0.37	0.37	0.95	-	-	0.97	1.00	1.92	0.99
16	35.08	0.15	0.07	44.65	b.d.l.	0.03	19.91	99.89	0.99	0.00	0.00	0.94	-	0.00	0.98	1.00	1.93	0.96
17	35.02	0.08	0.40	43.10	b.d.l.	0.05	20.90	99.59	0.99	0.00	0.01	0.91	-	0.00	1.03	1.00	1.93	0.88
18	33.68	0.56	0.71	43.89	b.d.l.	0.04	20.39	99.28	0.97	0.02	0.02	0.94	-	0.00	1.02	1.00	1.96	0.92
19	33.75	0.69	1.37	43.68	b.d.l.	b.d.l.	20.47	99.96	0.95	0.02	0.04	0.91	-	-	1.00	1.00	1.91	0.91
20	33.07	1.04	1.47	43.64	b.d.l.	0.02	20.01	99.26	0.93	0.03	0.04	0.92	-	0.00	0.98	1.00	1.90	0.93

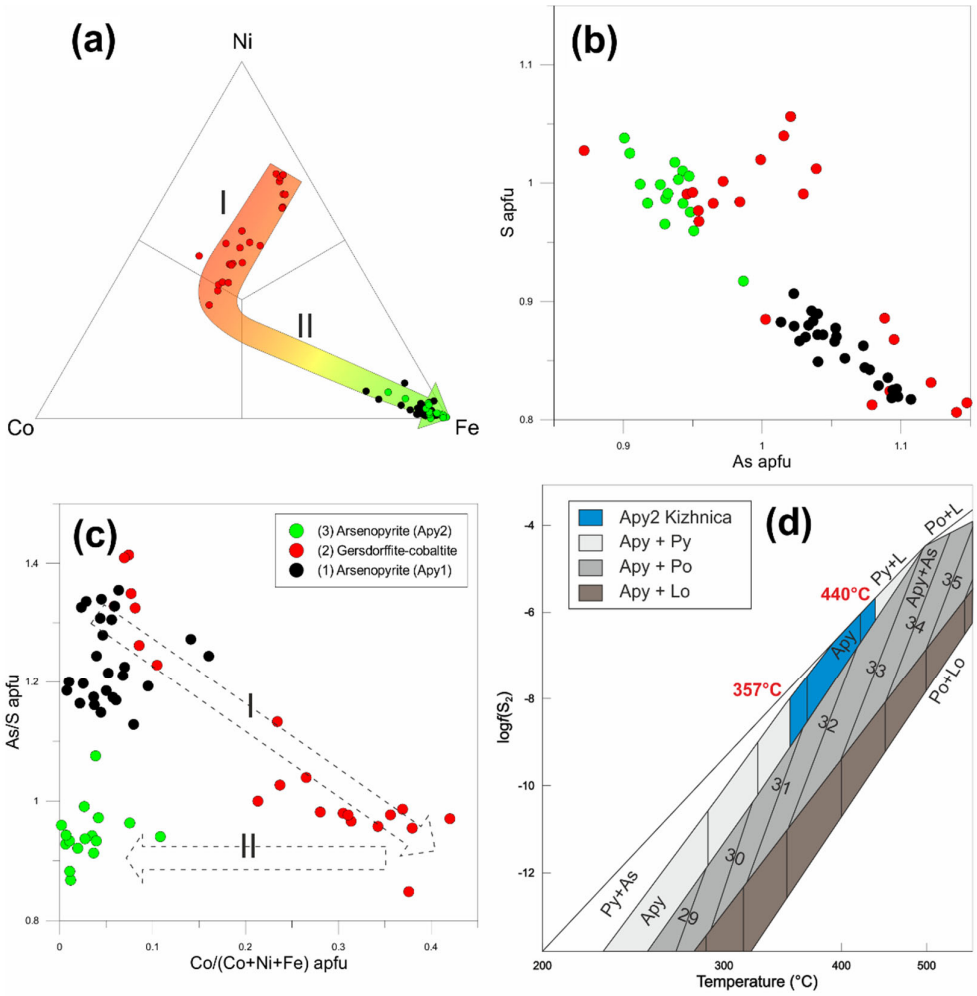

Figure 19. Plots showing the chemical composition of sulfarsenides from the Kizhnica hornfels: (**a**) ternary Ni-Co-Fe diagram; (**b**) binary S vs As (apfu) plot; (**c**) binary As/S vs Co/(Co + Ni+ Fe) plot; (**d**) activity of log*f*(S_2) and temperature projection of the stability field of arsenopyrite (Apy2) from Kizhnica hornfels after [65,66].

Arsenopyrite (Apy1) was the only ore mineral in samples from hornfels with sufficiently large crystals to be analyzed by LA-ICP-MS. Ablation patterns reveal the occurrence of different Bi sulfosalts inclusions and Mg-Fe amphiboles in arsenopyrite (Figure 20a–b). Enrichment of Bi (up to 313 ppm) and Pb (up to 4.7 ppm) is related to Bi sulfosalts inclusions, while Ti (up to 3500 ppm), Mn (up to 60 ppm), Cr (up to 120 ppm), and V (up to 120 ppm) are related to inclusions of Mg-Fe amphiboles (Table 4). The gold content in arsenopyrite is below the detection limit, while Au peaks in LA-ICP-MS spectra (Figure 20a,b) are related to native Au associated with bismuthinite inclusions. This indicates that gold-bearing fluids are related to the initial stages of Bi sulfosalts precipitation. Additionally, Pb and Bi peaks present in some LA-ICP-MS spectra are related to cannizzarite inclusions (Figure 20b).

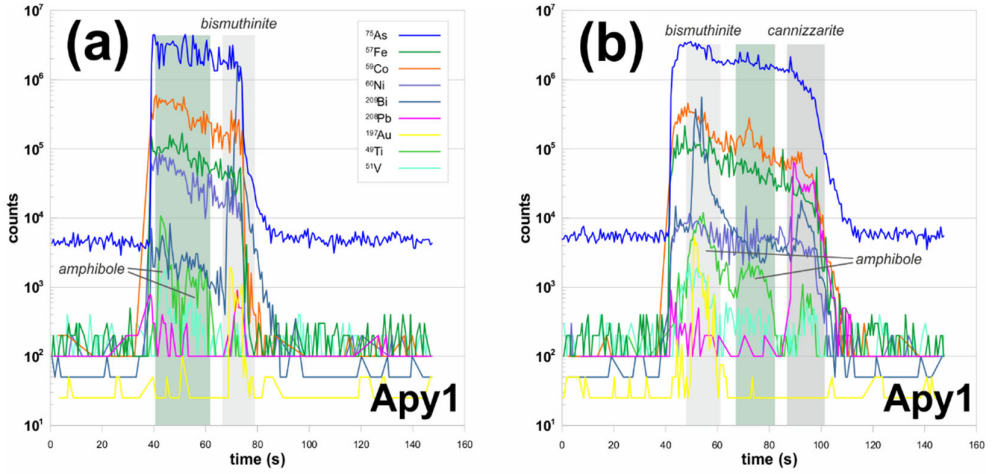

Figure 20. Selected time-resolved laser ablation ICP-MS depth profiles of early arsenopyrite (Apy1) and associated inclusions (highlighted in grey and green) from the Kizhnica hornfels: (**a**) spectra of Apy1; the spiky patterns of Bi and Au could suggest the occurrence of bismuthinite with gold, while Ti and V are related to amphibole inclusions; (**b**) spectra of Apy1; the similarly curved distribution patterns of Bi and Au could be related to inclusions of bismuthinite with gold, while inclusions of cannizzarite could be responsible for similar patterns of Pb and Bi; Ti and V are related to amphibole inclusions.

The second generation of sulfarsenides, less widespread in the studied rocks, is represented by gersdorffite and cobaltite forming a solid solution. They occur as small euhedral crystals up to 20 μm in size (Figure 18c) or bigger subhedral aggregates up to 100 μm in size. Euhedral crystals are often overgrown by younger chalcopyrite and Bi sulfosalts (Figure 14a) and display oscillatory zonality (Figure 18c). On the other hand, subhedral aggregates are characterized by patchy zonation. The formula of gersdorffite-cobaltite can be expressed as $(Ni_{0.32–0.69}Co_{0.06–0.42}Fe_{0.17–0.30})_{\sum 1}As_{0.92–1.15}S_{0.81–1.06}$ (Table 10). Most of the analyses fall on the gersdorffite field on the ternary gersdorffite-cobaltite-arsenopyrite diagram, and only two analyses can be classified as cobaltite (Figure 19a). The central parts of the crystals show the highest Ni concentrations; Co enriched zones are younger and occur at the edges of the crystals. Similar sulfarsenides trends are known in most Ni-Co hydrothermal mineralization worldwide [67]. The studied sulfarsenides show sequence: gersdorffite → cobaltite → younger arsenopyrite (Apy2). In addition to the above-mentioned cationic trend, there is also a smooth evolution observed at anionic positions and the As/S ratio. The As/S ratio in the second generation of sulfarsenides varies from 0.85–1.41 (Figure 19c). Gersdorffite with the highest Ni concentration is characterized by the highest As/S ratio similarly to Apy1 (~1.3) (Figure 19c). With the increase of Co in the sulfarsenides, a decrease in the As/S ratio is observed, ending with values similar to Apy2 (~1.0) (Figure 19c).

Younger arsenopyrite generation (Apy2) forms irregular zones up to 30 μm around early arsenopyrite crystals (Figure 18b). The formula of Apy2 can be expressed as $(Fe_{0.82–0.99}Co_{0.00–0.11}Ni_{0.00–0.07})_{\sum 1}As_{0.90–0.99}S_{0.92–1.04}$ (Table 10) and reveals the smallest variability at the cationic position among all generations of sulfarsenides (Figure 19a). Additionally, limited As ↔ S substitution was observed, while the As/S ratio was 0.87-1.08 (Figure 19c).

An arsenopyrite geothermometer based on As content in arsenopyrite [65,66] was used for determining the formation conditions. Six out of 43 chemical analyses of arsenopyrite from hornfels were selected, which satisfy the criteria: (1) Ni + Co + Sb ≤ 1 wt.%, and (2) the total does not deviate more than 2 wt.% from 100 wt. %. Only the youngest generation of arsenopyrite Apy2 fulfilled with these constraints. The As values of arsenopyrite fall in the "*pyrite+arsenopyrite*" field of the buffered assemblages involving arsenopyrite in the Fe-As-S system. Based on the obtained data, the precipitation of arse-

nopyrite should have occurred under the temperature of 357 °C ≤ T ≤ 440 °C and S_2 activity of −9.1 ≤ log $f(S_2)$ ≤ −6.2 (Figure 19d). For comparison, the conditions of arsenopyrite crystallization from Ni-Bi-Au paragenesis from Mazhiq were determined to be between 440–495 °C and −6 to −4.5 log $f(S_2)$ [19]. Similarly to sulfarsenides from Mazhiq, it is impossible to determine the direct crystallization temperatures of other sulfarsenides (gersdorffite and cobaltite) using their chemical composition. Previous experimental studies on sulfarsenides crystallization temperatures [68–71] have been performed in dry systems, and therefore, results cannot be used for hydrothermal conditions.

The evolution of sulfarsenides crystallization in the studied samples is presented on two graphs (Figure 19a,c). During the initial stage, early arsenopyrite (Apy1) was enriched in Co and Ni and crystallized with a high As/S ratio. As a result of hydrothermal solution activity, early arsenopyrite crystals were dissolved, remobilizing Ni and Co. Due to the widespread distribution of Apy1, despite containing only minor concentrations of Ni and Co, released metals were sufficient for crystallization of the younger generation of sulfarsenides (process I) forming initially gersdorffite with elevated As/S ratio and subsequently evolving towards cobalt-richer members and As/S ratio closer to 1.0 (Figure 19a,c). The evolution of sulfarsenides followed towards the iron member, stoichiometric arsenopyrite (Apy2) with As/S close to 1.0: process II (Figure 19a,c).

4.2.3. Associated Minerals

Chalcopyrite is widespread and occurs as aggregates up to 1 cm in size (Figure 14a) or small euhedral crystals (Figure 14d). Chalcopyrite co-crystallizes with base metal minerals (sphalerite, pyrrhotite, and pyrite) and Bi sulfosalts (bismuthinite and cannizzarite).

Native bismuth is common in the studied samples, forms tiny droplets up to 20 μm in size disseminated in calcite, and is rarely present as intergrowths with bismuthinite (Figure 14c). Native bismuth co-crystallizes with Bi sulfosalts and also crystallized on older arsenopyrite Apy1 (Figure 14f).

Native gold occurs as isolated crystals up to 5 μm, rarely in intergrowths with tetradymite and bismuthinite (Figure 14h), less frequently as inclusions in gersdorffite and arsenopyrite. Native gold from hornfels is relatively pure, only slightly enriched in Ag (up to 1.8 wt.%); the formula of native Au can be expressed as $Au_{0.96–0.98}Ag_{0.02–0.04}$. Previously described native Au in the Kizhnica area in listvenites from Badovc is enriched in Ag (12-13 wt.%) and Hg (~0.5 wt.%) [35].

Only 2 **tetradymite** crystals up to 5 μm were recognized in the studied samples, in association with native gold and bismuthinite (Figure 14h). The chemical formula of tetradymite (based on sum of all cations, average from 2 analyses) is $Bi_{1.85}Pb_{0.07}As_{0.03}Sb_{0.01}Fe_{0.04}Ag_{0.01}Te_{1.56}S_{0.99}$. Generally, it is Te depleted (1.59–1.54) and slightly Pb enriched (up to 0.13 apfu) in comparison to the theoretical formula Bi_2Te_2S.

Sphalerite is a minor constituent that occurs as irregular aggregates up to 200 μm in association with co-crystallizing chalcopyrite (Figure 14e). It is characterized by Fe admixtures up to 6.05 wt.%, and the sphalerite formula can be expressed as $(Zn_{0.90–0.92}Fe_{0.08–0.09})_{\sum 1}S_{1.03–1.04}$.

Pyrite forms euhedral or subhedral crystals up to 100 μm (Figure 14b,g). The chemical composition of pyrite corresponds to the ideal stoichiometry of this mineral phase with the formula: $Fe_{1.00}S_{1.94–2.04}$.

Pyrrhotite forms euhedral crystals up to 20 μm in size, rarely in intergrowths with chalcopyrite (Figure 14d).

Galena and **löllingite** are rare and form small crystals up to 10 μm in size, and both minerals were identified by EDS.

5. Discussion

The Kizhnica-Hajvalia-Badovc ore field is known for occurrences of polymetallic Pb-Zn-Ag deposits [4,20]. In the Kizhnica area, as in many ore fields within the Serbo-Macedonian metallogenic province, co-occurrence of Pb-Zn-Ag and Bi-Au±Cu mineralization is observed, and their position strongly depends on the distance from the intrusive complex which is the source of the hydrothermal fluids [17]. Bi-Au±Cu associations are typically related to contact metamorphic rocks–skarns and hornfels, as well as epithermal veinlets in volcanic rocks.

One of the regions where both mineralizations are observed is the Boranja ore field, Podrinje District, Serbia. Radosavljević et al. [17] described the zonal arrangement of several mineral associations: Fe-Cu(Bi) → Pb(Ag)-Zn → Sb(As) → CaF_2(Pb-Zn), with increasing distance from the Boranja granodiorite, with Cu-Bi-Au mineralization found within the Kram skarn zone, Boranja ore field [11]. Pb-Bi sulfosalts (bursaite, cannizzarite, cosalite, and aikinite), tetradymite, native gold, and native Bi are associated with sulfides disseminations in garnet-epidote skarn.

In the Rudnik ore field (Central Serbia), Pb-Zn-Ag coexists with Cu-Bi-W mineralization [72]. This polymetallic deposit comprises skarn-replacement and hydrothermal ore bodies, mainly hosted by sediments but occasionally also by dykes and sills and contact metamorphic rocks. Cu-Bi mineralization is represented by Bi-sulfosalts (e.g., galenobismutite, cosalite, vikingite, and gustavite) and native Bi [42,72].

Another important ore field is located in the Rogozna Mountain, on the border of Serbia and Kosovo where Pb(Ag)-Zn deposits associated with listvenites, e.g., Crnac [28,30,31], and Cu-Au mineralization related to the Karavansalija skarn occur [73]. The Cu–Au mineralization is predominantly hosted by skarns composed of epidote, grossular, zoisite, calcite, hedenbergite, and rarely quartz. The skarn sulfide mineralization is characterized by the presence of Fe-Cu-Zn sulfides, Fe-Ni sulfarsenides, Bi sulfosalts (bismuthinite and cosalite), and native Au [73].

The Stan Terg deposit, in central Kosovo, is an example of a classic carbonate replacement Pb-Zn-Ag deposit; moreover, it is the largest polymetallic deposit in Kosovo [15,16]. Copper-Bi mineralization associated with skarns occurs mainly in the NE parts of the deposit. Skarn association consists of hedenbergite, ilvaite, magnetite, pyrrhotite, pyrite, with minor chalcopyrite, sphalerite, galena, and quartz. In addition, bismuthinite, Bi-Pb sulfosalts, native Bi, and native Au are observed [15,16]. In addition, arsenopyrite-rich skarn-free mineralization with Bi-sulfotellurides, Bi- and Sb-sulfosalts, and galena in pyrite-pyrrhotite-rich was described by Kołodziejczyk et al. [15,16]. In the vicinity of the Stan Terg mine, two localities with Bi-Cu-Au mineralization were described in the Mazhiq area [19–21]. Epithermal veinlets in altered volcanic rocks, associated with Bi sulfosalts (bismuthinite, aikinite, krupkaite, and cosalite), chalcopyrite, pyrite, and native gold [19,21]. However, Bi-Au mineralization overprinted an earlier Fe-Ni sulfarsenide association observed in carbonate metasomatic-veins in listvenites in Mazhiq. Bi sulfosalts (bismuthinite and cosalite) occur here in association with galena and native Au [20,21]. Analyzing the spatial distribution of Pb-Zn-Ag mineralization, as well as Bi-Au mineralization in the Stan Terg area, it can be stated that the zonation in this area is NW-SE, with the epithermal Bi-Au mineralization associated with the proximity of volcanic complex east of Mazhiq, which may be the source of the mineralizing fluids.

Carbonate replacement Pb–Zn–Ag±Au mineralization in the Kamariza area, Lavrion, Greece, was described by Voudouris et al. [14,74]. Mineralization in the Kamariza area consists of sulfides and sulfarsenides; native metals (Au and Bi); and sulfosalts of Ag, Bi, Cu, Pb, As, and Sb (TGM, bismuthinite, lillianite homologues, and aikinite). Voudouris et al. [74] suggest that the assemblages gersdorffite + bismuthinite + native gold and native gold + native bismuth are evidence of the contribution of magmatic components to the hydrothermal system [74].

Bi-Cu ± Au mineralization in Kizhnica ore field form two different mineralization styles: (1) hydrothermal Cu-Bi veinlets in andesite and (2) disseminated contact type Bi-

Au-Cu-Te mineralization. In the Kizhnica andesite quarry, Bi sulfosalts are represented by bismuthinite, cosalite, akinite, and krupkaite, associated with pyrite, hematite, chalcopyrite, galena, sphalerite, and tetrahedrite group minerals. Disseminated Bi-Au-Cu-Te mineralization in hornfels consists of Bi sulfosalts (cannizzarite, bismuthinite, galenobismutite, cosalite), associated with sulfarsenides (arsenopyrite, gersdorffite, and cobaltite), base metal sulfides (chalcopyrite, pyrite, sphalerite, pyrrhotite, and galena), native gold, native bismuth, and tetradymite. The comparison of mineralogy from the studied Kizhnica locality with other mentioned Bi-Au ± Cu localities from the the Serbo-Macedonian metallogenic province supports the assumption that the Cu-Bi association consists mainly of chalcopyrite + members of bismuthinite-aikinite series + Bi-Pb sulfosalts (cosalite ± cannizzarite ± galenobismutite) + native Bi ± native Au.

Spatial distribution of major types of mineralization within the Kizhnica ore field (Bi-Cu ± Au in the east, Pb-Zn-Sb in the west, and Sb-As-Tl-Hg in the south) (Figure 2) suggests the proximity of volcanic/magmatic complex, which are also the main source of hydrothermal fluids responsible for the polymetallic mineralization over the entire ore field.

6. Conclusions

A new type of Bi-Cu ± Au mineralization was identified in the Kizhnica ore field (1) hydrothermal Cu-Bi veinlets from the andesite quarry and (2) disseminated contact type Bi-Au-Cu-Te mineralization in Kizhnica hornfels.

Various substitutions are observed in Bi-sulfosalts: $Bi^{3+} + \square \leftrightarrow Pb^{2+} + Cu^{+}$ substitution in members of the bismuthinite-aikinite series; $2(Cu^{+} + Ag^{+}) \leftrightarrow Pb^{2+}$ substitution and $Ag^{+} + Bi^{3+} \leftrightarrow 2Pb^{2+}$ lillianite type of substitution in cosalite; as well as heterovalent Pb–Bi substitution in cannizzarite. In general, galenobismutite, members of the bismuthinite-aikinite series, cannizzarite, and cosalite (from hornfels) are close to the theoretical formulae.

Sulfarsenides from the hornfels are mainly represented by arsenopyrite (2 generations) with an addiction of gersdorffite-cobaltite solid solution members. Crystallization started with early arsenopyrite 1 (enriched in Co-Ni), and then, these aggregates were leached, and subsequent formation of Ni-member (gersdorffite) occurred, followed by Co-member (cobaltite) and finally pure arsenopyrite 2.

Laser ablation inductively coupled plasma mass spectrometry (LA-ICP-MS) analyses of sphalerite, chalcopyrite, and tetrahedrite indicate increased content of In and Sn in the Kizhnica Bi-Cu-Au mineralization. In addition, LA-ICP-MS analyses in pyrites show the presence of many elements, e.g., Au, As, Co, Sb, Tl, Hg, Pb, and Bi related to the structure of pyrite or controlled by nano-inclusions.

The presence of Bi-Cu ± Au mineralization in the eastern part of the ore field suggests the proximity of volcanic/magmatic sources of mineralization that seem to be key to the origin of hydrothermal mineralization in the Kizhnica-Hajvalia-Badovc ore field.

Supplementary Materials: The following are available online at www.mdpi.com/article/10.3390/min11111223/s1, Table S1: Microprobe detection limits, Table S2: LA-ICP-MS data.

Author Contributions: Conceptualization, methodology S.M. and J.P.; sample collecting S.M., J.P., and B.H., microscopic analysis S.M.; EPMA, S.M.; LA-ICP-MS, S.M. and D.D.; investigation, S.M. and J.P.; writing—original draft preparation, S.M.; writing—review and editing, S.M., J.P., D.D., and B.H. All authors have read and agreed to the published version of the manuscript.

Funding: The research was funded by the Society of Economic Geologists Canada Foundation (SEGCF) Student Research Grant 2019 and the AGH University of Science and Technology statutory grant No. 11.11.140.320.

Acknowledgments: We are grateful to G. Kozub-Budzyń and A. Włodek from the Laboratory of Critical Elements at AGH-UST, Faculty of Geology, Geophysics and Environmental Protection for

help during EMPA data collection. We are also grateful to the anonymous reviewers, whose comments helped us to improve the manuscript.

Conflicts of Interest: The authors declare no conflicts of interest.

References

1. Baker, T. Gold ± copper endowment and deposit diversity in the Western Tethyan magmatic belt, southeast Europe: Implications for exploration. *Econ. Geol.* **2019**, *114*, 1237–1250. https://doi.org/10.5382/econgeo.4643.
2. Janković, S. The Carpatho-Balkanides and adjacent area: A sector of the Tethyan Eurasian metallogenic belt. *Miner. Depos.* **1997**, *32*, 426–433. https://doi.org/10.1007/s001260050110.
3. Borojević Šoštarić, S.B.; Cvetković, V.; Neubauer, F.; Palinkaš, L.A.; Bernroider, M.; Genser, J. Oligocene shoshonitic rocks of the Rogozna Mts. (Central Balkan Peninsula): Evidence of petrogenetic links to the formation of Pb–Zn–Ag ore deposits. *Lithos* **2012**, *148*, 176–195. https://doi.org/10.1016/j.lithos.2012.05.028.
4. Kołodziejczyk, J.; Pršek, J.; Voudouris, P.; Melfos, V.; Asllani, B. Sn-bearing minerals and associated sphalerite from lead-zinc deposits, Kosovo: An electron microprobe and LA-ICP-MS study. *Minerals* **2016**, *6*, 42. https://doi.org/10.3390/min6020042.
5. Frenzel, M.; Voudouris, P.; Cook, N.J.; Ciobanu, C.L.; Gilbert, S.; Wade, B.P. Evolution of a hydrothermal ore-forming system recorded by sulfide mineral chemistry: A case study from the Plaka Pb–Zn–Ag Deposit, Lavrion, Greece. *Miner. Depos.* **2021**, 1-22. https://doi.org/10.1007/s00126-021-01067-y.
6. Kroll, T.; Müller, D.; Seifert, T.; Herzig, P.M.; Schneider, A. Petrology and geochemistry of the shoshonite-hosted Skouries porphyry Cu–Au deposit, Chalkidiki, Greece. *Miner. Depos.* **2002**, *37*, 137–144. https://doi.org/10.1007/s00126-001-0235-6.
7. Serafimovski, T.; Stefanova, V.; Volkov, A.V. Dwarf copper-gold porphyry deposits of the Buchim-Damjan-Borov Dol ore district, Republic of Macedonia (FYROM). *Geol. Ore Depos.* **2010**, *52*, 179–195. https://doi.org/10.1134/S1075701510030013.
8. Stefanova, V.; Volkov, A.V.; Serafimovski, T.; Sidorov, A.A. Native gold from the Plavica epithermal deposit, Republic of Macedonia. *Dokl. Earth Sci.* **2013**, *451*, 818–823.
9. Siron, C.R.; Thompson, J.F.; Baker, T.; Darling, R.; Dipple, G. Origin of Au-rich carbonate-hosted replacement deposits of the Kassandra mining district, northern Greece: Evidence for Late Oligocene, structurally controlled, and zoned hydrothermal systems. *Econ. Geol.* **2019**, *114*, 1389–1414. https://doi.org/10.5382/econgeo.4664.
10. Voudouris, P.; Mavrogonatos, C.; Spry, P.G.; Baker, T.; Melfos, V.; Klemd, R.; Haase, K.; Repstock, A.; Djiba, A.; Bismayer, U.; et al. Porphyry and epithermal deposits in Greece: An overview, new discoveries, and mineralogical constraints on their genesis. *Ore Geol. Rev.* **2019**, *107*, 654–691. https://doi.org/10.1016/j.oregeorev.2019.03.019.
11. Radosavljević-Mihajlović, A.S.; Stojanovic, J.N.; Dimitrijevic, R.Z.; Radosavljević, S.A. Rare Pb-Bi sulfosalt mineralization from the Boranja orefield (Podrinje district, Serbia). *Neues Jb. Miner. Abh* **2007**, *184*, 217–224. https://doi.org/10.1127/0077-7757/2007/0094.
12. Serafimovski, T.; Tasev, G.; Stefanova, V. Rare mineral phases related with major sulphide minerals in the Bučim porphyry copper deposit, R. Macedonia. *Geol. Maced.* **2013**, *27*, 43–54.
13. Voudouris, P.C.; Spry, P.G.; Mavrogonatos, C.; Sakellaris, G.A.; Bristol, S.K.; Melfos, V.; Fornadel, A.P. Bismuthinite derivatives, lillianite homologues, and bismuth sulfotellurides as indicators of gold mineralization in the Stanos shear-zone related deposit, Chalkidiki, Northern Greece. *Can. Miner.* **2013**, *51*, 119–142. https://doi.org/10.3749/canmin.51.1.119.
14. Voudouris, P.; Mavrogonatos, C.; Rieck, B.; Kolitsch, U.; Spry, P.G.; Scheffer, C.; Tarantola, A.; Vanderhaeghe, O.; Galanos, E.; Melfos, V.; et al. The gersdorffite-bismuthinite-native gold association and the skarn-porphyry mineralization in the Kamariza mining district, Lavrion, Greece. *Minerals* **2018**, *8*, 531. https://doi.org/10.3390/min8110531.
15. Kołodziejczyk, J.; Pršek, J.; Melfos, V.; Voudouris, P.C.; Maliqi, F.; Kozub-Budzyń, G. Bismuth minerals from the Stan Terg deposit (Trepça, Kosovo). *Neues Jb. Miner. Abh* **2015**, *192*, 317–333. https://doi.org/10.1127/njma/2015/0288.
16. Kołodziejczyk, J.; Pršek, J.; Voudouris, P.C.; Melfos, V. Bi-sulphotellurides associated with Pb-Bi-(Sb±Ag, Cu, Fe) sulphosalts: An example from the Stan Terg deposit in Kosovo. *Geol. Carpath.* **2017**, *68*, 366–381. https://doi.org/10.1515/geoca-2017-0025.
17. Radosavljević, S.A.; Stojanović, J.N.; Radosavljević-Mihajlović, A.S.; Kašić, V.D. Polymetallic mineralization of the Boranja orefield, Podrinje Metallogenic District, Serbia: Zonality, mineral associations and genetic features. *Perdiod Miner.* **2013**, *82*, 61–87. https://doi.org/10.2451/2013PM0004.
18. Buerger, R.; Giroux, G. *NI 43-101 Technical Report on the Slivovo Gold–Silver Project*; Avrupa-Minerals: Pristina, Kosovo, 2016; pp. 1–117.
19. Mederski, S.; Pršek, J.; Asllani, B.; Kozub-Budzyń, G. Bi-sulphosalts from the Mazhiq, Stan Terg area, Kosovo. In Proceedings of the 5th Central-European Mineralogical Conference and 7th Mineral Sciences in the Carpathians Conference, Banska Štiavnica, Slovakia, 26–30 June 2018.
20. Mederski, S.; Wojsław, M.; Pršek, S.; Majzlan, J.; Kiefer, S.; Asllani, B. A geochemical study of gersdorffite from the Trepça Mineral Belt, Vardar Zone, Kosovo. *J. Geosci.* **2021**, *66*, 97–115. http://dx.doi.org/10.3190/jgeosci.322.
21. Węgrzynowicz, J.; Pršek, J.; Mederski, S.; Asllani, B.; Kwiecień, K.; Kanigowski, J. Pb−Bi(−Cu) and Pb−Sb sulfosalts from Stan Terg area, Kosovo. In *Proceedings of the Life with Ore Deposits on Earth 15th Biennial SGA Meeting, Advances in Understanding Hydrothermal Processes, Glasgow, Scotland, 27–30 August 2019;* Volume 1; University of Glasgow Publicity Services: Glasgow, Scotland, 2019; pp. 380–383.

22. Janković, S. The principal metallogenic features of the Kopaonik District. In Proceedings of the Geology and Metallogeny of the Kopaonik Mt Symposium, Belgrade, Serbia, 19–22 June 1995, pp. 79–101.
23. Elezaj, Z. Geodynamic evolution of Kosovo during the Triassic and Jurassic. *Yerbilimleri* **2009**, *30*, 113–126.
24. Strmić Palinkaš, S.; Palinkaš, L.A.; Renac, C.; Spangenberg, J.E.; Lüders, V.; Molnar, F.; Maliqi, G. Metallogenic model of the Trepca Pb-Zn-Ag Skarn deposit, Kosovo: Evidence from fluid inclusions, rare earth elements, and stable isotope data. *Econ. Geol.* **2013**, *108*, 135–162. http://dx.doi.org/10.2113/econgeo.108.1.135.
25. Hyseni, M.; Durmishaj, B.; Fetahaj, B.; Shala, F.; Berisha, A.; Large, D. Trepça Ore Belt and Stan Terg mine—Geological overview and interpretation, Kosovo (SE Europe). *Geologija* **2010**, *51*, 87–92. http://dx.doi.org/10.5474/geologija.2010.006.
26. Strmić Palinkaš, S.A.; Palinkaš, L.; Mandić, M.; Roller-Lutz, Z.; Pécskay, Z.; Maliqi, G.; Bermanec, V. Origin and K-Ar age of the phreatomagmatic breccia at the Trepča Pb-Zn-Ag skarn deposit, Kosovo: Implications for ore-forming processes. *Geol. Croat.* **2016**, *69*, 121–142. https://doi.org/10.4154/GC.2016.10.
27. Féraud, J.; Deschamps, Y. *French Scientific Cooperation 2007–2008 on the Trepça Lead-Zinc-Silver Mine and the Gold Potential of Novo Brdo/Artana Tailings (Kosovo)*; BRGM Report No RP-57204-FR.; BRGM: Orléans, France, 2009; pp. 1–99.
28. Radosavljević, S.A.; Stojanović, J.N.; Vuković, N.S.; Radosavljević-Mihajlović, A.S.; Kašić, V.D. Low-temperature Ni-As-Sb-S mineralization of the Pb (Ag)-Zn deposits within the Rogozna Orefield, Serbo-Macedonian Metallogenic Province: Ore mineralogy, crystal chemistry and paragenetic relationships. *Ore Geol. Rev.* **2015**, *65*, 213–227. https://doi.org/10.1016/j.oregeorev.2014.09.029.
29. Dangić, A. Minor element distribution between galena and sphalerite as a geothermometer—Application to two lead-zinc areas in Yugoslavia. *Econ. Geol.* **1985**, *80*, 180–183. http://dx.doi.org/10.2113/gsecongeo.80.1.180.
30. Borojević Šoštarić, S.B.; Palinkaš, L.A.; Topa, D.; Spangenberg, J.E.; Prochaska, W. Silver–base metal epithermal vein and listwaenite types of deposit Crnac, Rogozna Mts., Kosovo. Part I: Ore mineral geochemistry and sulfur isotope study. *Ore Geol. Rev.* **2011**, *40*, 65–80. https://doi.org/10.1016/j.oregeorev.2011.05.002.
31. Borojević Šoštarić, S.B.; Palinkaš, L.A.; Neubauer, F.; Hurai, V.; Cvetković, V.; Roller-Lutz, Z.; Mandić, J.; Genser, J. Silver-base metal epithermal vein and listwanite hosted deposit Crnac, Rogozna Mts., Kosovo, part II: A link between magmatic rocks and epithermal mineralization. *Ore Geol. Rev.* **2013**, *50*, 98–117. https://doi.org/10.1016/j.oregeorev.2012.10.005.
32. Kołodziejczyk, J.; Prsek, J.; Asllani, B.; Maliqi, F. The paragenesis of silver minerals in the Pb-Zn Stan Terg deposit, Kosovo: An example of precious metal epithermal mineralization. *Geol. Geophys. Environ.* **2016**, *42*, 19–29. https://doi.org/10.7494/geol.2016.42.1.19.
33. Durmishaj, B.; Hyseni, S.; Kelmendi, M. Geochemical association of the sulfides of lead-zinc mineralization in Trepça mineral belt-Kizhnica mine, Kosovo. *Int. J. Geol. Agric.* **2015**, *3*, 1–4.
34. Durmishaj, B.; Hyseni, S.; Tashko, A. The main geochemical association of the sulfides of lead-zinc mineralization in Trepça Mineral Belt- Hajvalia mine, Kosovo. *ARPN J. Eng. Appl. Sci.* **2014**, *9*, 1376–1380.
35. Mederski, S.; Pršek, J.; Hincyngier, K. Pb−Zn−Sb−Ni−Au mineralization from the Kizhnica area, central Kosovo: New data on the listwaenite type mineralization. In *Proceedings of the Life with Ore Deposits on Earth 15th Biennial SGA Meeting, Magmatic Sulfide and Oxide Systems; Gold—From Orogenesis to Alluvial; Supergenes, Gems and Non-Metallic Ores, Glasgow, Scotland, 27–30 August 2019;* Volume 2; University of Glasgow Publicity Services: Glasgow, Scotland, 2019; pp. 834–837.
36. Westner, K. Roman Mining and Metal Production Near the Antique City of ULPIANA (Kosovo). Ph.D. Thesis, Goethe-Universität, Frankfurt, Germany, 2017.
37. Mederski, S.; Pršek, J.; Dimitrova, D. Geochemistry of tetrahedrite group minerals from the Janjevo Cu-Bi-Ag(Pb,W) locality: Results of EPMA and LA-ICP-MS investigations. *Acta Miner. Petrogr.* **2021**, *11*, 29.
38. Guillong, M.; Meier, D.L.; Allan, M.M.; Heinrich, C.A.; Yardley, B.W.D. Appendix A6: SILLS: A MATLAB-based program for the reduction of laser ablation ICP-MS data of homogeneous materials and inclusions. In *Laser Ablation ICP–MS in the Earth Sciences: Current Practices and Outstanding Issues*; Sylvester, P., Eds.; Mineralogical Association of Canada Short Course 40: Vancouver, BC, Canada, 2008; pp. 328–333.
39. Topa, D.; Makovicky, E.; Paar, W.H. Composition ranges and exsolution pairs for the members of the bismuthinite–aikinite series from Felbertal, Austria. *Can. Miner.* **2002**, *40*, 849–869. https://doi.org/10.2113/gscanmin.40.3.849.
40. Pršek, J.; Ozdín, D.; Sejkora, J. Eclarite and associated Bi sulfosalts from the Brezno-Hviezda occurrence (Nízke Tatry Mts, Slovak Republic). *Neues Jb. Miner. Abh* **2008**, *185*, 117–130. https://doi.org/10.1127/0077-7757/2008/0112.
41. Topa, D.; Makovicky, E. The crystal chemistry of cosalite based on new electron-microprobe data and single-crystal determinations of the structure. *Can. Miner.* **2010**, *48*, 1081–1107. https://doi.org/10.3749/canmin.48.5.1081.
42. Stojanovic, J.N.; Radosavljević, S.A.; Karanović, L.; Cvetković, L. Mineralogy of WPbBi ores from Rudnik Mt., Serbia. *Neues Jb. Miner. Abh* **2006**, *182*, 299–306. https://doi.org/10.1127/0077-7757/2006/0053.
43. Buzatu, A.; Damian, G.; Dill, H.G.; Buzgar, N.; Apopei, A.I. Mineralogy and geochemistry of sulfosalts from Baia Sprie ore deposit (Romania)—New bismuth minerals occurrence. *Ore Geol. Rev.* **2015**, *65*, 132–147. https://doi.org/10.1016/j.scitotenv.2015.10.139.
44. George, L.L.; Biagioni, C.; Lepore, G.O.; Lacalamita, M.; Agrosì, G.; Capitani, G.C.; Bonaccorsia, E.; d'Acapito, F. The speciation of thallium in (Tl, Sb, As)-rich pyrite. *Ore Geol. Rev.* **2019**, *107*, 364–380. https://doi.org/10.1016/j.oregeorev.2019.02.031.
45. Ciobanu, C.L.; Cook, N.J.; Pring, A.; Brugger, J.; Danyushevsky, L.V.; Shimizu, M. 'Invisible gold' in bismuth chalcogenides. *Geochim. Cosmochim. Acta* **2009**, *73*, 1970–1999.

46. Kołodziejczyk, J. Mineralogical and Geochemical Diversity Within the Stan Terg Deposit, Kosovo. Ph.D. Thesis, AGH University of Science and Technology, Kraków, Poland, 2016.
47. Cook, N.J.; Ciobanu, C.L.; Pring, A.; Skinner, W.; Shimizu, M.; Danyushevsky, L.; Melcher, F. Trace and minor elements in sphalerite: A LAICPMS study. *Geochim. Cosmochim. Acta* **2009**, *73*, 4761–4791. https://doi.org/10.1016/j.gca.2009.05.045.
48. Cook, N.J.; Sundblad, K.; Valkama, M.; Nygård, R.; Ciobanu, C.L.; Danyushevsky, L. Indium mineralisation in A-type granites in southeastern Finland: Insights into mineralogy and partitioning between coexisting minerals. *Chem. Geol.* **2011**, *284*, 62–73. https://doi.org/10.1016/j.chemgeo.2011.02.006.
49. Cook, N.J.; Ciobanu, C.L.; Brugger, J.; Etschmann, B.; Howard, D.L.; de Jonge, M.D.; Paterson, D. Determination of the oxidation state of Cu in substituted Cu-In-Fe-bearing sphalerite via μ-XANES spectroscopy. *Am. Miner.* **2012**, *97*, 476–479. https://doi.org/10.2138/am.2012.4042.
50. Murakami, H.; Ishihara, S. Trace elements of Indium-bearing sphalerite from tin-polymetallic deposits in Bolivia, China and Japan: A femto-second LA-ICPMS study. *Ore Geol. Rev.* **2013**, *53*, 223–243. https://doi.org/10.1016/j.oregeorev.2013.01.010.
51. Belissont, R.; Boiron, M.C.; Luais, B.; Cathelineau, M. LA-ICP-MS analyses of minor and trace elements and bulk Ge isotopes in zoned Ge-rich sphalerites from the Noailhac–Saint-Salvy deposit (France): Insights into incorporation mechanisms and ore deposition processes. *Geochim. Cosmochim. Acta* **2014**, *126*, 518–540. https://doi.org/10.1016/j.gca.2013.10.052.
52. Frenzel, M.; Hirsch, T.; Gutzmer, J. Gallium, germanium, indium, and other trace and minor elements in sphalerite as a function of deposit type—a meta-analysis. *Ore Geol. Rev.* **2016**, *76*, 52–78. https://doi.org/10.1016/j.oregeorev.2015.12.017.
53. Xu, J.; Cook, N.J.; Ciobanu, C.L.; Li, X.; Kontonikas-Charos, A.; Gilbert, S.; Lv, Y. Indium distribution in sphalerite from sulfide–oxide–silicate skarn assemblages: A case study of the Dulong Zn–Sn–In deposit, Southwest China. *Miner. Depos.* **2021**, *56*, 307–324. https://doi.org/10.1007/s00126-020-00972-y.
54. Biagioni, C.; George, L.L.; Cook, N.J.; Makovicky, E.; Moëlo, Y.; Pasero, M.; Sejkora, J.; Stanley, C.J.; Welch, M.D.; Bosi, F. The tetrahedrite group: Nomenclature and classification. *Am. Miner.* **2020**, *105*, 109–122. https://doi.org/10.2138/am-2020-7128.
55. George, L.L.; Cook, N.J.; Ciobanu, C.L. Minor and trace elements in natural tetrahedrite-tennantite: Effects on element partitioning among base metal sulphides. *Minerals* **2017**, *7*, 17. https://doi.org/10.3390/min7020017.
56. Topa, D.; Makovicky, E.; Dittrich, H. The crystal structure of 7H: 12Q cannizzarite from Vulcano, Italy. *Can. Miner.* **2010**, *48*, 483–495. https://doi.org/10.3749/canmin.48.3.483.
57. Borisov, S.V.; Pervukhina, N.V.; Magarill, S.A.; Kuratieva, N.V.; Bryzgalov, I.A.; Mozgova, N.N.; Chaplygin, I.V. The crystal structure of (Cd, In)-rich cannizzarite from Kudriavy volcano, Iturup island, Kuriles, Russia. *Can. Miner.* **2012**, *50*, 387–395. https://doi.org/10.3749/canmin.50.2.387.
58. Matzat, E. Cannizzarite. *Acta Cryst.* **1979**, *35*, 133–136.
59. Makovicky, E.; Hyde, B.G. Non-commensurate (misfit) layer structures. *Struct. Bond.* **1981**, *46*, 101–170.
60. Mozgova, N.N.; Kuzmina, O.V.; Organova, N.I.; Laputina, I.P. New data on sulphosalt assemblages at Vulcano (Italy). *Rend. Soc. Ital. Miner. Petrol.* **1985**, *40*, 277–283.
61. Borodaev, Y.S.; Garavelli, A.; Garbarino, C.; Grillo, S.M.; Mozgova, N.N.; Organova, N.I.; Trubkin, N.V.; Vurro, F. Rare sulfosalts from Vulcano, Aeolian islands, Italy. III. Wittite and cannizzarite. *Can. Miner.* **2000**, *38*, 23–34. https://doi.org/10.2113/gscanmin.38.1.23.
62. Izumino, Y.; Nakashima, K.; Nagashima, M. Cuprobismutite group minerals (cuprobismutite, hodrušhite, kupčíkite and paděraite), other Bi–sulfosalts and Bi–tellurides from the Obari mine, Yamagata Prefecture, Japan. *J. Miner. Petrol. Sci.* **2014**, *109*, 177–190. https://doi.org/10.2465/jmps.140129.
63. Topa, D.; Makovicky, E.; Criddle, A.J.; Paar, W.H.; Balić-Žunić, T. Felbertalite, $Cu_2Pb_6Bi_8S_{19}$, an new mineral species from Felbertal, Salzburg Province, Austria. *Eur. J. Miner.* **2001**, *13*, 961–972. https://doi.org/10.1127/0935-1221/2001/0013-0961.
64. Garavelli, A.; Laviano, R.; Vurro, F. Sublimate deposition from hydrothermal fluids at the Fossa crater-Vulcano, Italy. *Eur. J. Miner.* **1997**, *9*, 423–432. https://doi.org/10.1127/ejm/9/2/0423.
65. Kretschmar, U.; Scott, S.D. Phase relations involving arsenopyrite in the system Fe-As-S and their application. *Can. Miner.* **1976**, *14*, 364–386.
66. Sharp, Z.D.; Essene, E.J.; Kelly, W.C. A re-examination of the arsenopyrite geobarometry: Pressure considerations and applications to natural assemblages. *Can. Miner.* **1985**, *23*, 517–534.
67. Scharrer, M.; Kreissl, S.; Markl, G. The mineralogical variability of hydrothermal native element-arsenide (five-element) associations and the role of physicochemical and kinetic factors concerning sulfur and arsenic. *Ore Geol. Rev.* **2019**, *113*, 103025. https://doi.org/10.1016/j.oregeorev.2019.103025.
68. Yund, R.A. The system Ni-As-S; phase relations and mineralogical significance. *Am. J. Sci.* **1962**, *260*, 761–782.
69. Klemm, D.D. Synthesen und Analysen in den Dreiecksdiagrammen FeAsS-CoAsS-NiAsS und FeS_2-CoS_2-NiS_2. *Neues Jb. Miner. Abh* **1965**, 205-255. https://doi.org/10.1127/njma/103/1965/205.
70. Hem, S.R.; Makovicky, E. The system Fe–Co–Ni–As–SI Phase relations in the (Fe,Co,Ni)$As_{0.5}S_{1.5}$ section at 650 and 500 °C. *Can. Miner.* **2004**, *42*, 43–62. https://doi.org/10.2113/gscanmin.42.1.43.
71. Hem, S.R.; Makovicky, E. The system Fe–Co–Ni–As–S. II. Phase relations in the (Fe,Co,Ni)$As_{1.5}S_{0.5}$ section at 650 and 500 °C. *Can. Miner.* **2004**, *42*, 63–86. https://doi.org/10.2113/gscanmin.42.1.63.
72. Stojanović, J.N.; Radosavljević, S.A.;Tošović, R.D.; Pačevski, A.M.; Radosavljević-Mihajlović, A.S.; Kašić, V.D.; Vuković, N.S. A review of the Pb-Zn-Cu-Ag-Bi-W polymetallic ore from the Rudnik orefield, Central Serbia. *Geol. An. Balk. Poluos.* **2018**, *79*, 47–69. https://doi.org/10.2298/GABP1879047S.

73. Budinov, Z.D.; Yonezu, K.; Tindell, T.; Gabo-Ratio, J.A.; Milutinovic, S.; Boyce, A.J.; Watanabe, K. Copper–gold skarn mineralization at the Karavansalija ore zone, Rogozna Mountain, Southwestern Serbia. *Resour. Geol.* **2015**, *65*, 328–344. https://doi.org/10.1111/rge.12075.
74. Voudouris, P.; Melfos, V.; Spry, P.G.; Bonsall, T.A.; Tarkian, M.; Solomos, C. Carbonate-replacement Pb–Zn–Ag±Au mineralization in the Kamariza area, Lavrion, Greece: Mineralogy and thermochemical conditions of formation. *Miner. Petrol.* **2008**, *94*, 85–106. https://doi.org/10.1007/s00710-008-0007-4.